Cell Reports

Article

Distinct roles for NF-κB in hematopoietic stem cells and the bone marrow milieu in promoting hematopoietic aging

Graphical abstract

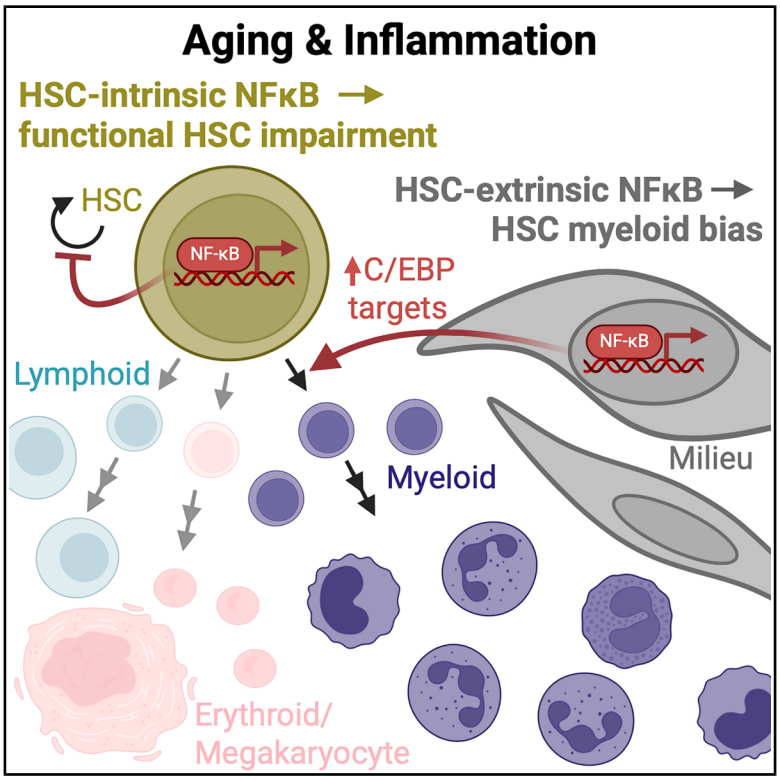

Highlights

- Hematopoietic-extrinsic NF-κB activity is sufficient for myeloid-biased hematopoiesis
- The inflamed bone marrow milieu directs epigenomic reprogramming of HSCs
- NF-κB activity within HSCs is associated with quiescence but not myeloid bias
- Hematopoietic-intrinsic NF-κB activity drives functional HSC impairment

Authors

Jennifer J. Chia, Apeksha Singh, Yu-Sheng Lin, ..., Jennifer K. King, Dinesh S. Rao, Alexander Hoffmann

Correspondence

ahoffmann@ucla.edu

In brief

Chia et al. find that inflammatory NF-κB signaling serves distinct functions within HSCs vs. the bone marrow milieu: HSC-intrinsic NF-κB promotes HSC quiescence and limits function, while an inflamed milieu directs HSC epigenomic reprogramming toward myeloid bias. Omics signatures of both HSC-intrinsic and milieu inflammation occur in aged mice and humans.

Chia et al., 2025, Cell Reports *44*, 116193
September 23, 2025
https://doi.org/10.1016/j.celrep.2025.116193

CellPress

Cell Reports

CellPress
OPEN ACCESS

Article

Distinct roles for NF-κB in hematopoietic stem cells and the bone marrow milieu in promoting hematopoietic aging

Jennifer J. Chia,[1,2,3,4] Apeksha Singh,[4,5] Yu-Sheng Lin,[4] Noa Popko,[4] David Mastro,[4] Yi Liu,[4,8] Tiffany Tran,[1] Jennifer K. King,[6] Dinesh S. Rao,[1,2,3] and Alexander Hoffmann[2,3,4,7,9,*]

[1]Department of Pathology and Laboratory Medicine, David Geffen School of Medicine, University of California, Los Angeles, Los Angeles, CA, USA
[2]Jonsson Comprehensive Cancer Center, University of California, Los Angeles, Los Angeles, CA, USA
[3]Broad Stem Cell Research Center, University of California, Los Angeles, Los Angeles, CA, USA
[4]Department of Microbiology, Immunology, and Molecular Genetics, University of California, Los Angeles, Los Angeles, CA, USA
[5]UCLA/Caltech Medical Scientist Training Program, University of California, Los Angeles, Los Angeles, CA, USA
[6]Department of Medicine, David Geffen School of Medicine, University of California, Los Angeles, Los Angeles, CA, USA
[7]Institute for Quantitative and Computational Biosciences, University of California, Los Angeles, Los Angeles, CA, USA
[8]Present address: DeepKinase Biotechnologies Ltd., Beijing, China
[9]Lead contact
*Correspondence: ahoffmann@ucla.edu
https://doi.org/10.1016/j.celrep.2025.116193

SUMMARY

Hematopoietic aging is characterized by chronic inflammation associated with myeloid bias, hematopoietic stem cell (HSC) accumulation, and functional HSC impairment. Yet it remains unclear how inflammation promotes aging phenotypes. Nuclear factor κB (NF-κB) both responds to and directs inflammation, and we present an experimental model of elevated NF-κB activity ("inhibitor of κB deficient" [IκB^{-}]) to dissect its role in hematopoietic aging phenotypes. We find that while elevated NF-κB activity is not sufficient for HSC accumulation, HSC-autonomous NF-κB activity impairs their functionality, leading to reduced bone marrow reconstitution. In contrast, myeloid bias is driven by the IκB^{-} proinflammatory bone marrow milieu, as observed functionally, epigenomically, and transcriptomically. A single-cell RNA sequencing (scRNA-seq) HSPC labeling framework enables comparisons with aged murine and human HSC datasets, documenting an association between HSC-intrinsic NF-κB activity and quiescence but not myeloid bias. These findings delineate separate regulatory mechanisms that underlie the three hallmarks of hematopoietic aging, suggesting that they are specifically and independently therapeutically targetable.

INTRODUCTION

Hematopoietic aging phenotypes include chronic inflammation, bias of hematopoietic output toward myeloid lineages and away from lymphoid fates, and hematopoietic stem cell (HSC) dysfunction.[1,2] Aged HSCs accumulate in number yet display increased quiescence and impaired responses to regenerative cues.[2–4] Furthermore, HSCs and their multipotent progenitor (MPP) progeny (together, hematopoietic stem and progenitor cells [HSPCs]) display myeloid bias during diverse physiologic and pathologic inflammatory responses.[1,5] While chronic inflammation is tightly linked with hematopoietic aging, whether it is a driver or consequence of myeloid bias, HSC functional decline, or HSC accumulation remains unclear.

Nuclear factor κB (NF-κB) is a ubiquitous regulator of inflammation but is also downstream of inflammatory stimuli with roles in development, stress responses, and cancer.[6–8] Interestingly, there is increased NF-κB activity in aged HSCs.[9] The NF-κB signaling system, composed of IκB kinase (IKK) signal integration complexes, inhibitor of κB (IκB) negative regulators, and NF-κB transcription factor (TF) dimers, is activated by tissue damage and inflammatory molecules (e.g., damage-associated molecular patterns [DAMPs], pathogen-associated molecular patterns [PAMPs], and cytokines), culminating in NF-κB nuclear translocation and gene transcription.[6] Key transcriptional targets include cytokines (e.g., *Tnf* and *Il1a*), chemokines (e.g., *Ccl5*), and growth factors (e.g., *Csf3*), in addition to cell cycle, apoptosis, and cell stress pathway components.[6] Furthermore, the NF-κB system participates in the control of other signaling pathways, such as mitogen-activated protein kinase (MAPK), phosphatidylinositol 3 (PI3)-kinase, transforming growth factor beta (TGF-β), Wnt, and type I interferon, that also impact hematopoiesis.[10] Both HSCs and their niches are altered in hematopoietic aging, yet there remains controversy regarding the contributions of each compartment to aging phenotypes.[1,11] The diverse functions of NF-κB across tissue types raise the question of whether NF-κB-mediated signaling within both HSCs and their niches may each contribute to hematopoietic aging.

While perturbations of the NF-κB system have shown its importance in hematopoiesis, existing models each have critical limitations.[12] Mice with IKK and NF-κB-inducing kinase (NIK) mutations show bone marrow failure, but importantly, both IKK and NIK have pleiotropic targets outside the NF-κB pathway.[10,12,13] *Nfkb1*$^{-/-}$ mice display features of premature aging; however, the biological consequences may be due to dysregulated NF-κB, type I interferon, or dysregulated MAPK signaling.[14] *Relb*$^{-/-}$ mice have a complex inflammatory, autoimmune, and immunodeficiency phenotype that is so severe that they are not suitable for aging studies.[15] In contrast, NF-κB activation achieved by reducing IκB-mediated sequestration of NF-κB dimers in the cytoplasm is a direct and NF-κB system-specific approach. Knockout mice for *Nfkbia* encoding IκBα show granulocytosis but die shortly after birth, while *Nfkbia*$^{+/-}$ heterozygous mice show no phenotype due to compensation by other IκB family members,[16] limiting the utility of these mice for *in vivo* studies.

Here, we present a genetic model of inflammatory NF-κB dysregulation termed IκB^{-} (*Nfkbia*$^{+/-}$*Nfkbib*$^{-/-}$*Nfkbie*$^{-/-}$) to study the causal relationship between inflammation, myeloid bias, HSC accumulation, and HSC functional impairment in hematopoietic aging. We demonstrate the utility of this model as young IκB^{-} mice display myeloid bias and an inflammatory bone marrow milieu, similar to aged wild-type (WT) mice. Transplantation experiments in conjunction with epigenomic and transcriptomic analyses reveal inflammatory milieu-directed myeloid bias that is separable from HSC-intrinsic NF-κB activity, quiescence, and functional impairment. Together, these findings delineate separate roles for inflammatory NF-κB signaling in the bone marrow milieu and within HSCs in driving different aspects of aging-associated hematopoietic decline.

RESULTS

Experimentally elevated NF-κB drives myeloid-biased hematopoiesis, similar to aging

To assess NF-κB control in hematopoietic progenitors of aged mice, we used an mVenus-RelA reporter previously generated in our laboratory.[17] In this mouse, the mVenus fluorescent signal indicates the abundance of RelA protein, which is the NF-κB subunit most critical for inflammatory responses.[8] In young mice (2–3 months), we found that HSPC subsets, as phenotypically delineated by Pietras and colleagues[18] (Figure S1A), vary in NF-κB RelA abundance, with megakaryocyte-erythroid-biased MPP2 cells showing the highest expression, while the lowest is seen in short-term HSCs (ST-HSCs; also proposed to represent an MPP rather than a true stem cell[19]) (Figures 1A, 1B, and S1B). Upon aging (18–22 months), RelA protein is increased in long-term HSC (LT-HSC), ST-HSC, myeloid-biased MPP3, and lymphoid-biased MPP4 subsets (Figures 1A, S1B, and S1C).

To test whether elevated NF-κB activity may be a sufficient driver of aging-associated myeloid bias, HSC functional impairment, and HSC accumulation, we bred mice harboring knockout alleles for genes encoding IκB family members, resulting in a compound IκB-deficient strain termed IκB^{-} (*Nfkbia*$^{+/-}$*Nfkbib*$^{-/-}$*Nfkbie*$^{-/-}$).[16,20,21] This combination of genetic perturbations results in reduced cytoplasmic sequestration of NF-κB dimers, leading to the increased nuclear presence of NF-κB and target gene expression. Accordingly, young IκB^{-} mice showed significant increases in soluble bone marrow inflammatory mediators over young WT controls. Indeed, the cytokine profile was remarkably similar to the inflammatory milieu observed in aged WT mice (Figure 1C).

Bone marrow cellularity was similar between young IκB^{-} mice and controls; however, the total number of HSPCs was increased in IκB^{-} (Figure 1D). This was predominantly due to an increased abundance of megakaryocyte/erythroid-biased MPP2s and myeloid-biased MPP3s, without a change in the number of lymphoid-biased MPP4s (Figure 1D). ST-HSCs were reduced in IκB^{-} mice, while LT-HSC abundance was unchanged compared to young WT controls (Figure 1D). These HSPC subset differences were appreciated as both absolute cell numbers (Figure 1D) and as the percentage of composition of the HSPC compartment (Figure S1D). Aged mice showed similar increases in MPP2s and MPP3s as IκB^{-}, and additional changes were noted, including a reduction in total bone marrow cellularity, a decrease in MPP4s, and an increase in LT-HSCs (Figures 1D and S1D), consistent with established literature in aged mice.[1,2] LT-HSC expression of CD150 has been associated with lineage biases. CD150^{high} myeloid-biased HSCs (myHSCs) accumulate with aging,[22] which we also observed in our aged murine cohort but not in IκB^{-} mice (Figure S1E), consistent with the lack of HSC accumulation in this model.

Mature granulocytosis was observed by histology and flow cytometry in both young IκB^{-} and aged WT mice compared with young WT controls (Figures S1F and S1G). In the peripheral blood, young IκB^{-} mice showed fewer circulating B cells (further explored by Y.-S. L., V. Alonso, Y.L., Y. Tang, A.S., A. Mehta, J. King, M. Paing, N. Salomis, H. Grimes, et al., unpublished data), increased myeloid cell subsets, and no difference in T cell abundances (Figures S1H and S1I). These findings were similar to, though more pronounced than, those observed in aged WT mice (Figure S1I) and indicate myeloid bias among mature immune effector cells.

Together, these results indicate that experimentally driving ubiquitous proinflammatory NF-κB signaling is sufficient for myeloid-biased hematopoiesis as in aged mice but does not lead to aging-associated HSC accumulation.

Hematopoietic-cell-extrinsic NF-κB activity is sufficient to drive myeloid bias

The striking abundance of soluble inflammatory mediators in IκB^{-} and aged bone marrow (Figure 1C) raises the possibility that they may be responsible for driving myeloid bias. These soluble factors may be produced by either hematopoietic cells or non-hematopoietic cells. To distinguish between these possibilities, we generated bone marrow chimeric mice by transplanting WT donor bone marrow into IκB^{-} recipients or WT controls (Figure 2A). This strategy allowed us to measure how elevated NF-κB activity in the radio-resistant, hematopoietic cell-extrinsic compartment affects WT donor cells. Transplant recipients of both genotypes showed excellent chimerism 15 weeks post-transplant (>97%; Figures 2B and S2A), when donor HSCs show stable hematopoietic reconstitution.[23,24] Experimental hematopoietic-extrinsic NF-κB dysregulation in IκB^{-} recipients

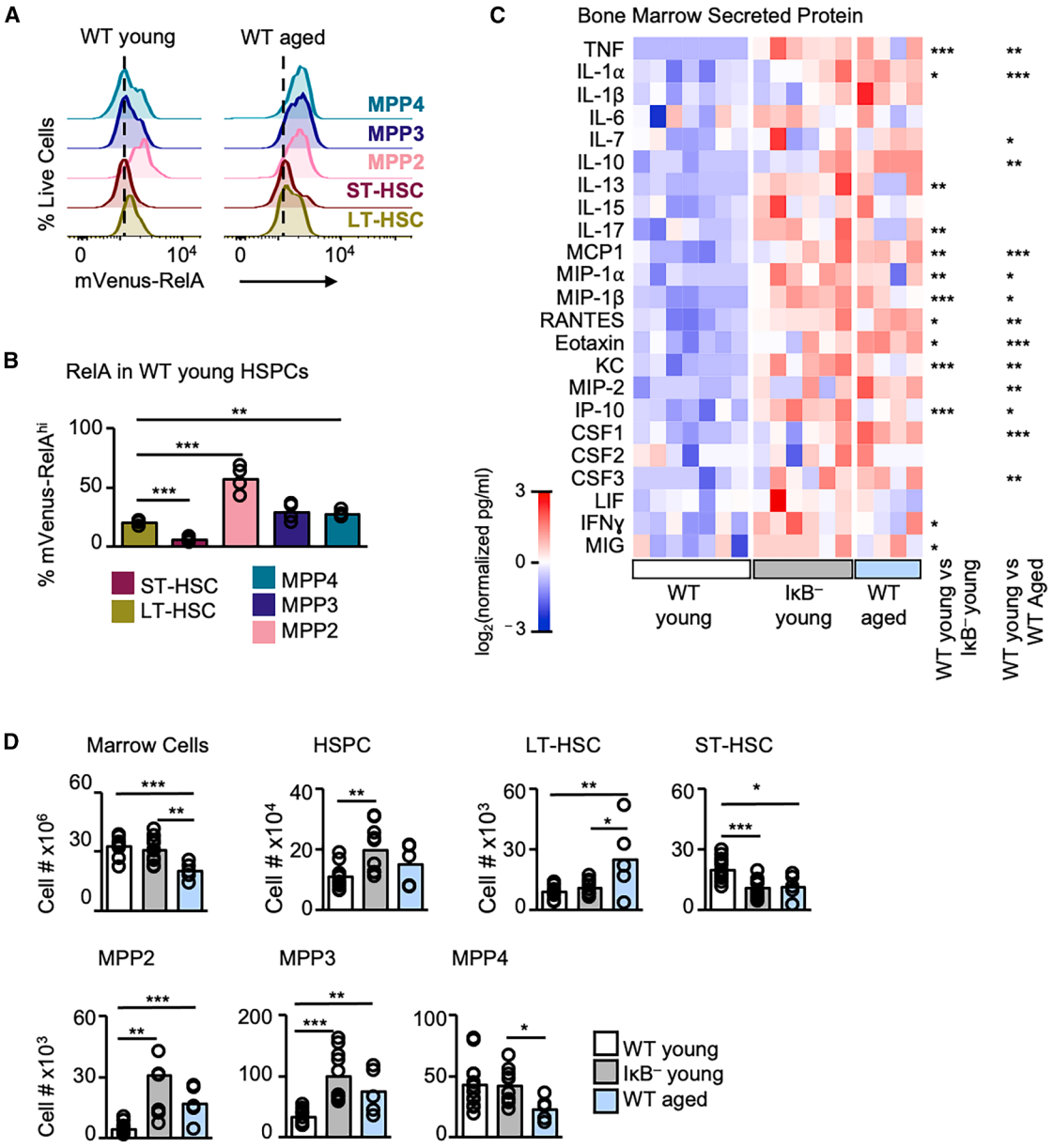

Figure 1. IκB⁻ mouse model of NF-κB dysregulation has an inflamed bone marrow and myeloid-biased hematopoiesis, similar to aged mice

(A) mVenus-RelA fluorescence normalized to cell counts in the indicated HSPC subsets; representative of $n = 4–5$.

(B) Quantification of RelA^{hi} young WT cells; statistics compare LT-HSC to other HSPC subsets.

(C) Secreted protein in bone marrow supernatant measured by Luminex, normalized to mean of WT young samples, per assay plate; $n = 4–7$.

(D) Total bone marrow, total HSPC, and HSPC subset cell numbers by flow cytometry; $n = 5–12$.

Unpaired Student's two-tailed t test p values: $^{*}p < 0.05$, $^{**}p < 0.01$, and $^{***}p < 0.001$. See also Figure S1.

resulted in unchanged bone marrow cellularity and total HSPC numbers between recipient genotypes (Figure 2C); however, myeloid-biased MPP3s were increased among WT donor cells from IκB⁻ recipients measured by absolute number (Figure 2C) and as a proportion of the entire HSPC compartment (Figure S2B) compared to controls. A minor increase was also noted in MPP2s, and ST-HSC numbers showed a down trend ($p = 0.05$) (Figures 2C and S2B), revealing similar though weaker effects on these populations compared with non-transplanted IκB⁻ mice. Bone marrow mature granulocytosis was seen by histology and flow cytometry (Figures S2C and S2D), and peripheral blood immunophenotyping showed increased myeloid cells (Figure S2E), indicating myeloid bias among mature immune effector cells. Concordantly, bone marrow supernatant showed increased protein levels of the myeloid growth factors CSF3 and eotaxin[25] (Figures S2F). These results

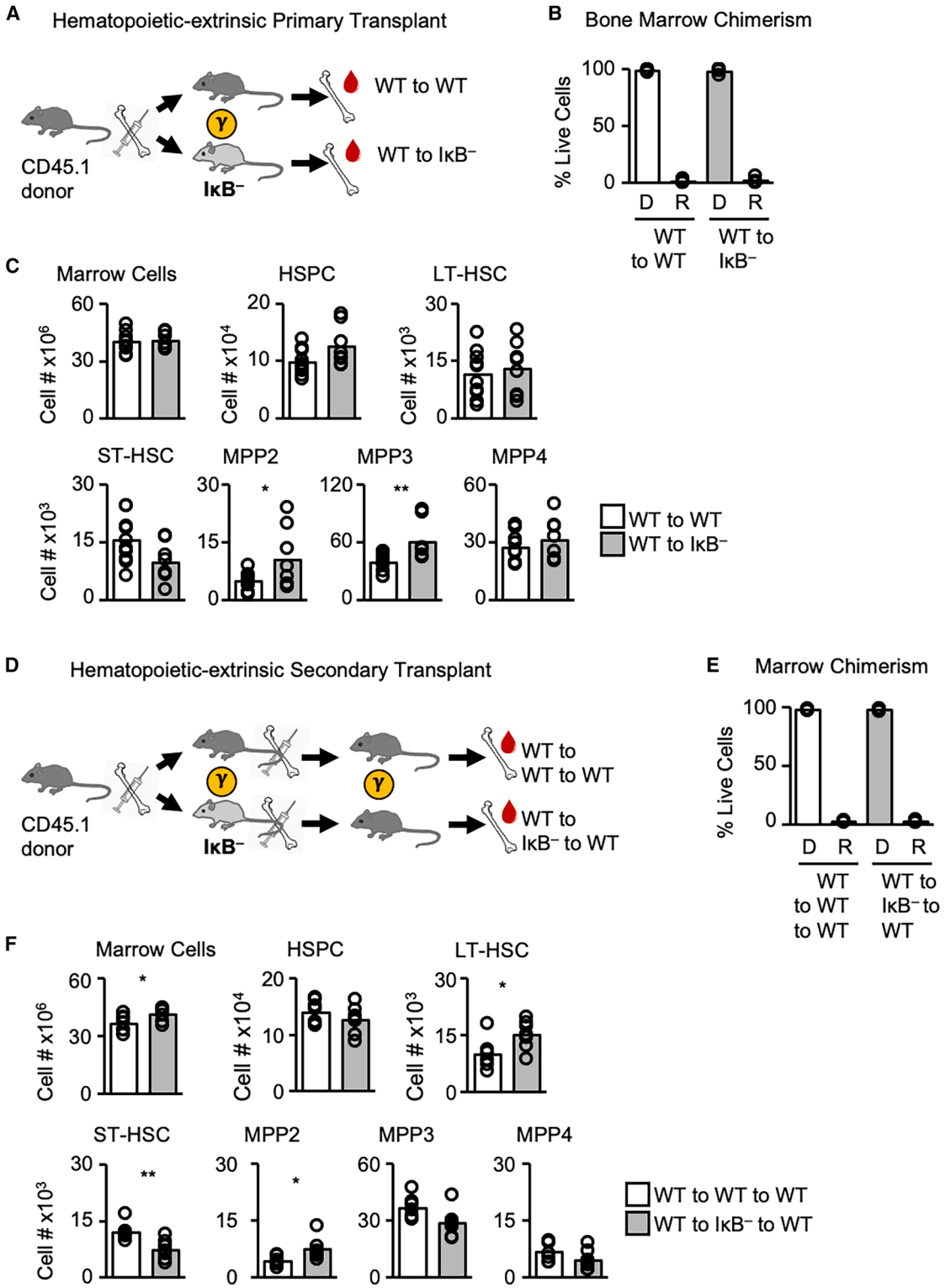

Figure 2. Hematopoietic-extrinsic inflammatory signals are sufficient to drive myeloid-biased hematopoiesis

(A) Primary transplant schematic.

(B) Bone marrow chimerism at 15 weeks. D, donor; R, recipient.

(C) Donor marrow, HSPC, and HSPC subset cell numbers.

(D) Secondary transplant schematic.

(legend continued on next page)

indicate that myeloid bias of stably engrafted WT donor cells in IκB^{-} recipients was similar to that in non-transplanted IκB^{-} mice. Therefore, NF-κB activity restricted to the radio-resistant compartment is sufficient for myeloid bias.

We next tested the durability of milieu-directed myeloid bias upon re-transplantation into a WT bone marrow milieu. Secondary transplantation of WT marrow conditioned in IκB^{-} primary recipients for 15 weeks into young WT secondary recipients (Figures 2D, 2E, and S2G) led to a remarkable resolution of MPP3 and bone marrow granulocyte bias after 16 weeks (Figures 2F and S2H–S2J). Together, these experiments demonstrate that HSC-extrinsic NF-κB activity is sufficient to drive myeloid-biased hematopoiesis. However, NF-κB-driven inflammatory signals in the milieu must be persistent to maintain myeloid bias in the bone marrow, as HSPC myeloid bias is reversible upon return into a non-dysregulated bone marrow milieu.

The inflamed bone marrow milieu directs epigenomic reprogramming of HSCs

We next asked whether epigenomic changes may underlie the HSPC myeloid bias induced in WT cells by the inflamed IκB^{-} bone marrow milieu. We performed the assay for transposase accessible chromatin with sequencing (ATAC-seq) in flow-cytometry-sorted LT-HSC (HSC), MPP2, MPP3, and MPP4 populations from WT-to-WT or WT-to-IκB^{-} bone marrow chimeric mice (Figure S3A), identifying 13,910 consensus peaks of accessible chromatin among 3 biological replicates. We confirmed that peaks were appropriately larger for regions expected to be open in all samples (e.g., *Gapdh*) than for regions expected to be closed in all samples (e.g., *Pbpb*) and that peaks showed appropriate cell-type specificity (e.g., *Pf4* in MPP2s) (Figure 3A).

To identify differentiation-associated changes in chromatin accessibility for each progenitor lineage, we used differential accessibility analysis between each MPP subset vs. HSCs, performed separately for cells from WT and IκB^{-} recipients (Figures S3B and S3C). In these differentially accessible regions (DARs), we then assessed TF motif enrichment in megakaryocyte/erythroid-biased (Mk/Er) MPP2s, myeloid-biased (My) MPP3s, and lymphoid-biased (Ly) MPP4s (Figure 3B).[26–29] In contrast to WT-recipient controls, IκB^{-}-recipient MPP3 vs. HSC DARs showed little enrichment for CCAAT/enhancer-binding protein (C/EBP) motifs (Figure 3B), which was surprising given the myeloid-biased phenotype in IκB^{-}-recipient mice and C/EBP's prominent role in myeloid differentiation.[27,30] While this analysis related DARs of MPPs vs. HSCs within the same recipient genotype, we next directly compared IκB^{-}- vs. WT-recipient DARs for each HSPC subset to identify changes in chromatin accessibility driven by the inflammatory milieu (Figures S3D and 3C). This analysis revealed a dramatic enrichment of C/EBP motifs among IκB^{-}-recipient HSCs and moderate enrichments in MPP3 and MPP4 populations (Figure 3C). A similar pattern was noted for PU.1 (Figure S3E), which instructs both myeloid and early lymphoid programs,[31] but not for megakaryocyte/erythroid-associated nor lymphoid-specific TF motifs (Figure 3C). We then performed Gene Ontology (GO) analysis on the top 25 enriched TF motifs in IκB^{-}- vs. WT-recipient DARs (Figures S3B and S3D). The top TF motifs showed significant enrichment in GO terms related to transcriptional regulation for all populations, as expected; furthermore, multiple terms related to myeloid development and differentiation were significantly enriched, particularly in HSCs and MPP4s (Figure S3F).

We next identified specific chromatin regions associated with the myeloid lineage that become prematurely accessible in WT HSCs transplanted into an inflamed IκB^{-} milieu. Among 595 myeloid-specific DARs in WT recipients (defined as more accessible in WT-recipient MPP3s vs. HSCs), a distinct cluster of 115 DARs showed higher peak counts in IκB^{-}-recipient HSCs than controls (Figures S3B and 3D). C/EBPα and C/EBPβ have well-established roles in steady-state and emergency myelopoiesis, respectively, and C/EBPδ is implicated in granulocyte specification and function.[27] Furthermore, C/EBPα and C/EBPβ are pioneer factors that can open heterochromatin, thereby facilitating changes in transcriptional programs, either independently of or synergistically with PU.1.[32] Thus, we asked whether these myeloid-associated DARs may overlap with *bona fide* C/EBP binding events, which were defined from publicly available chromatin immunoprecipitation with sequencing datasets of differentiated myeloid cells.[33–35] Indeed, we found that the 115 myeloid regions prematurely accessible in IκB^{-}-recipient HSCs showed a high overlap with C/EBP binding events, as did total WT-recipient myeloid-specific MPP3 vs. HSC DARs (595), while negative control WT-recipient HSC-specific DARs (434) did not (Figure 3E), confirming that newly accessible regions in HSCs from an IκB^{-} milieu are enriched in *bona fide* C/EBP binding sites. Regions with high C/EBP overlap also showed higher peak counts, indicating increased chromatin accessibility at these C/EPB binding sites (Figure 3F). Together, these findings identify inappropriate or premature accessibility for C/EBPs and their binding in HSCs in an inflammatory IκB^{-} milieu as a form of epigenomic reprogramming.

The inflamed bone marrow milieu redirects the gene expression program of HSCs

Next, we asked whether WT HSPCs from an inflammatory IκB^{-} milieu may also show transcriptional features of myeloid bias. We performed single-cell RNA sequencing (scRNA-seq) on flow-cytometry-sorted HSPCs from WT-to-WT or WT-to-IκB^{-} bone marrow chimeric mice (Figure S4A). To identify HSPCs that relate to the individually sorted subsets in our ATAC-seq analysis, we developed a logistic-regression-based cell labeling model. This model generated HSPC subset labels from bulk-sorted LT-HSC, ST-HSC, MPP2, MPP3, and MPP4 microarray data, which were then filtered by an independent bulk-sorted scRNA-seq dataset, both of which used the same phenotypic

(E) Bone marrow chimerism at 16 weeks.
(F) Donor bone marrow, HSPC, and HSPC subset cell numbers.
(A–C) n = 9–11, 3 transplant batches. (D–F) n = 7, one transplant batch. Unpaired Student's two-tailed t test p values; *$p < 0.05$, **$p < 0.01$, and ***$p < 0.001$. See also Figure S2.

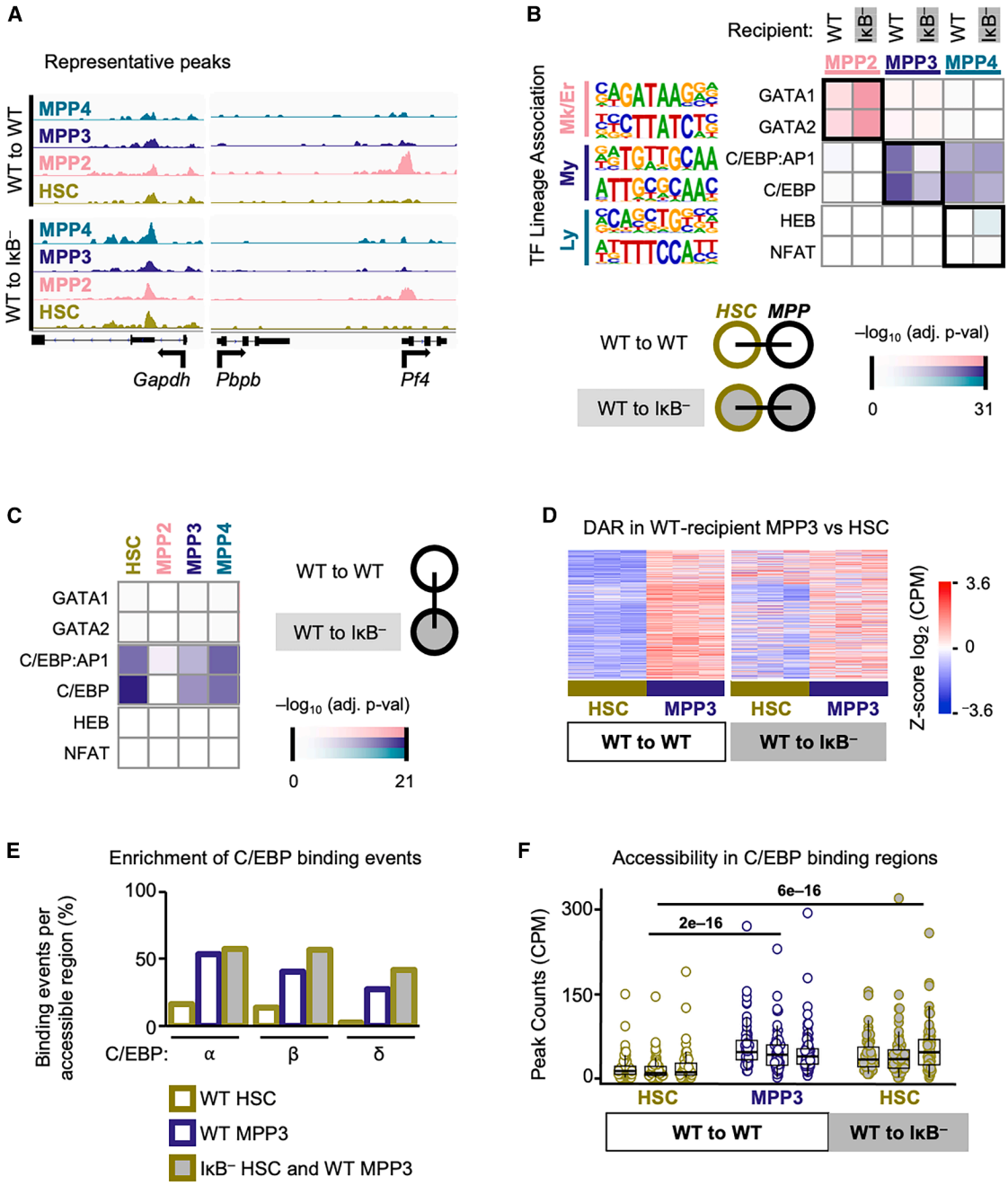

Figure 3. In an inflammatory milieu, HSCs undergo chromatin reorganization that results in increased accessibility for myeloid-priming C/EBP transcription factors

ATAC-seq analysis from hematopoietic-extrinsic primary transplants.

(A) Peak tracks corresponding to regions expected to be open (*Gapdh*), closed (*Pbpb*), or population specific (*Pf4*); representative of $n = 3$.

(B) Transcription factor (TF) motif enrichment among more accessible differentially accessible chromatin regions (DARs) in the specified MPP population vs. HSCs for each recipient genotype (inset schematic).

(C) TF motif enrichment in more accessible DARs in IκB$^-$ recipients vs. WT recipients (inset schematic) for each population.

(D) *z* scored CPM-normalized peak counts in the more accessible 595 DARs in WT-recipient MPP3 vs. WT-recipient HSCs; $n = 3$.

(E) Overlap between published C/EBP binding events and ATAC-seq DARs accessible in WT-recipient HSCs but not WT-recipient MPP3s ("WT HSCs"), in WT-recipient MPP3s but not WT-recipient HSCs ("WT MPP3s"), or in WT-recipient MPP3s and IκB$^-$-recipient HSCs but not WT-recipient HSCs ("IκB$^-$ HSCs and WT MPP3s").

(F) CPM-normalized peak counts in "IκB$^-$ HSC and WT MPP3" regions overlapping with C/EBP binding events for the indicated populations and all replicates. Statistics in (B) and (C) are Benjamini-Hochberg (BH)-adjusted *p* values calculated via Homer zero or one occurrence per sequence (ZOOPS) scoring; statistics in (F) were calculated with Wilcoxon rank-sum test. See also Figure S3.

cell surface markers as our ATAC-seq sorting strategy.[18,36] In test scRNA-data, cell-type labels were assigned as one of the five HSPC cell types that showed the highest transcriptomic correspondence between test and reference data (Figure S5). Labeling our hematopoietic-extrinsic transplant scRNA-seq data resulted in more MPP3-labeled cells from IκB$^-$ recipients than WT-recipient controls (Figures 4A, 4B, and S4B–S4D), consistent with flow cytometry phenotyping. We first evaluated the expression of genes nearest the accessible C/EBP binding events identified in Figures 3D–3F. These transcripts were increased among the differentially expressed genes (DEGs) from positive control WT-recipient MPP3s vs. LT-HSCs, as expected (Figure 4C, *x* axis), and were also higher in LT-HSCs from IκB$^-$ recipients vs. controls (Figure 4C, *y* axis), confirming the increased transcription of most C/EBP target genes in HSCs conditioned in an inflamed environment. We next sought to perform transcript abundance analysis while retaining single-cell resolution. To do so, we calculated rank-based single-cell gene set enrichment scores,[37] yielding a scoring metric that indicates how highly expressed a set of genes is within each cell. For ATAC-accessible C/EBP target genes, C/EBP target single-cell gene set scores were higher in IκB$^-$-recipient HSCs than controls (Figure 4D), consistent with the DEG-based analysis. These findings confirmed increased transcript abundance for genes in C/EBP binding regions that were prematurely accessible in HSCs from an inflamed IκB$^-$ milieu.

We next evaluated broader transcriptional features of myeloid bias. Expression of 31 myeloid lineage- and maturation-associated genes[38] encoding myeloid TFs, growth factor receptors, and functional proteins (Table S1) was increased in LT-HSC from IκB$^-$ vs. WT recipients in both DEG (Figure 4E) and single-cell gene set scoring (Figure 4F) approaches. Furthermore, myeloid-associated genes showed higher single-cell scores among IκB$^-$-recipient MPPs than WT-recipient controls (Figure 4F). To confirm our findings with an orthogonal, non-overlapping gene set, we used 49 CSF3R-response genes from the NCI Cytosig database,[39] including *Ctsb*, *Nampt*, and *Timp1* (Table S1). Concordantly, single-cell gene set scores were higher for CSF3R-response genes in HSCs and non-MPP3 progenitors from IκB$^-$ recipients (Figure 4G). Lymphoid-associated transcripts were evaluated using a gene set of 11 lymphoid lineage-associated genes,[40] including *Dntt*, *Rag1*, and *Ikzf1* (Table S1). Lymphoid scores were unchanged in HSCs and were reduced in MPP3s and MPP4s from IκB$^-$ recipients compared to WT recipients (Figure 4H). Together, these three myeloid-associated, CSF3R-responsive, and lymphoid-associated gene sets contain <100 genes; however, our cell-type labeling model incorporates expression data of 7,563 genes to resolve lineage-associated features among transcriptomically similar stem and progenitor cells. Thus, we next examined the distributions of cell-type assignment probabilities from our labeling model. This revealed that among MPP3-labeled cells, IκB$^-$-recipient cells had higher MPP3 assignment probabilities than controls (Figure S4E). Conversely, among MPP4-labeled cells, IκB$^-$-recipient MPP4s had lower MPP4 assignment probabilities (Figure S4E). Together, these findings identify transcriptional myeloid bias in LT-HSCs and MPPs conditioned in the inflammatory IκB$^-$ milieu.

Milieu-directed transcriptional bias of HSCs in aged mice and humans

To determine whether transcriptional signatures of HSCs in an inflammatory milieu occur in naturally aged individuals, we evaluated publicly available scRNA-seq datasets from murine HSPCs and human CD34-positive cells.[41–44] We applied our cell labeling model to each dataset to ensure fair comparisons between them (Figures 5A, 5B, and S6A) and confirmed the suitability of our labeling method for human data using species-specific reference genes[45] (Figure S6B). In the absence of chromatin accessibility data, we computationally inferred TF activity from scRNA-seq using the decoupleR tool that leverages independent gene regulatory and transcriptomic databases.[46] Comparing scRNA-seq DEGs of aged vs. young LT-HSCs from mice and humans, we found a combination of increased myeloid TF activity and reduced lymphoid TF activity,[47,48] pointing to an overall myeloid-biased TF repertoire (Figure 5C). To assess transcriptional myeloid potentiation and lymphoid decline in a single metric, a bias score was calculated as the difference between the CSF3R-response (or myeloid-associated) single-cell gene set enrichment score and the lymphoid-associated score. The resultant CSF3R-bias scores were strongly increased in LT-HSCs from all aged datasets (Figure 5D), and myeloid-bias scores were increased in 3 of 4 datasets (Figure 5E). Slight differences between these scores may reflect early vs. later events in myeloid commitment, as LT-HSCs from hematopoietic-extrinsic transplantation experiments had higher scores for CSF3R responses than for myeloid-associated genes (Figures 4F and 4G). These findings indicate transcriptional myeloid bias in aged HSCs from mice and humans, similar to murine HSCs from an inflamed IκB$^-$ milieu.

Aged HSCs show transcriptomic signatures of quiescence or myeloid bias but not both

HSCs remain in quiescence, a poised, reversible G0 state, until they receive an activation cue to enter the cell cycle.[3] This results in a long-lived pool of HSCs that can maintain multilineage hematopoietic potential throughout the lifespan, while progenitor proliferation contributes to the bulk of hematopoietic output.[1] Importantly, quiescence is now recognized as a spectrum rather than a binary on/off state, and increased quiescence has been associated with aging and HSC accumulation, though the mechanism remains unclear.[1,50] Aged HSCs were more abundant than young HSCs in all 3 scRNA-seq datasets that had no further cell sorting or selection (Mitchell et al.,[41] Hérault et al.,[42] and Ainciburu et al.[43] datasets; Figure S6C), consistent with age-associated HSC accumulation[4,51] (Figure 1E). To explore the depth of quiescence in aged HSCs, we calculated single-cell gene set scores using 73 genes with well-established roles in quiescence, including *Ccnd3*, *Ezh1*, and *Cdc42* (Table S1).[49,52] Indeed, aged LT-HSCs showed higher quiescence scores than young LT-HSCs for all datasets with HSC accumulation (Figure 5F). Thus, both transcriptional myeloid bias and increased quiescence signatures are consistently observed in aged HSCs from mice and humans.

We next leveraged the single-cell resolution of these data to examine the relationship between transcriptomic myeloid bias and quiescence states. On a per-cell basis, we surprisingly observed no correlation between myeloid bias and quiescence scores (Figure S6D). We then asked how highly quiescent

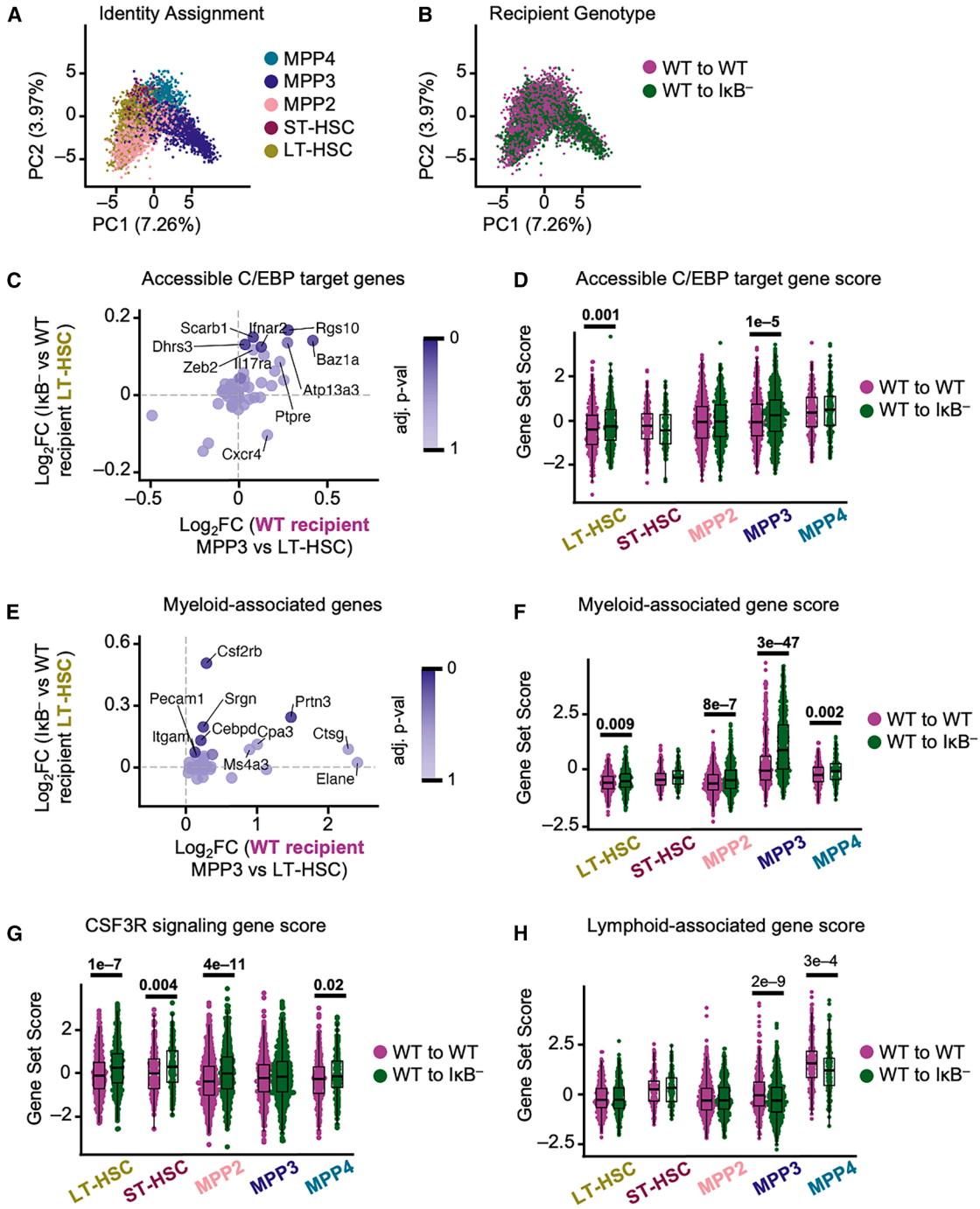

Figure 4. HSPCs in an inflammatory milieu show a myeloid-biased transcriptional state

(A and B) scRNA-seq cells from hematopoietic-extrinsic primary transplants labeled by cell identity assignment (A) or by recipient genotype (B), plotted in principal-component analysis (PCA) space defined by expression of 115 genes with known functions in hematopoiesis.

(C and D) Expression of genes corresponding to "IκB⁻ HSC and WT MPP3" DARs that overlap with C/EBP binding events (as in Figures 3E and 3F) expressed as population-level differentially expressed genes (DEGs) (*x* axis shows positive control WT-recipient MPP3s vs. LT-HSCs, and *y* axis shows experimental LT-HSCs from IκB⁻ recipients vs. controls) (C) or expressed as rank-based single-cell gene set enrichment scores (D).

(E and F) Expression of 31 myeloid-associated genes[38] by population DEGs (*x* axis shows positive control WT-recipient MPP3s vs. LT-HSCs, and *y* axis shows experimental LT-HSCs from IκB⁻ recipients vs. controls) (E) or as single-cell gene set scores (F).

(G and H) Single-cell set scores for CSF3R-response genes[39] (G) and lymphoid-associated genes[40] (H).

(C and E) BH-adjusted color scale *p* values correspond to *y* axis DEGs. (D–F) Wilcoxon rank-sum test *p* values; bold typeface indicates an increase in mean vs. control. See also Figures S4 and S5 and Table S1.

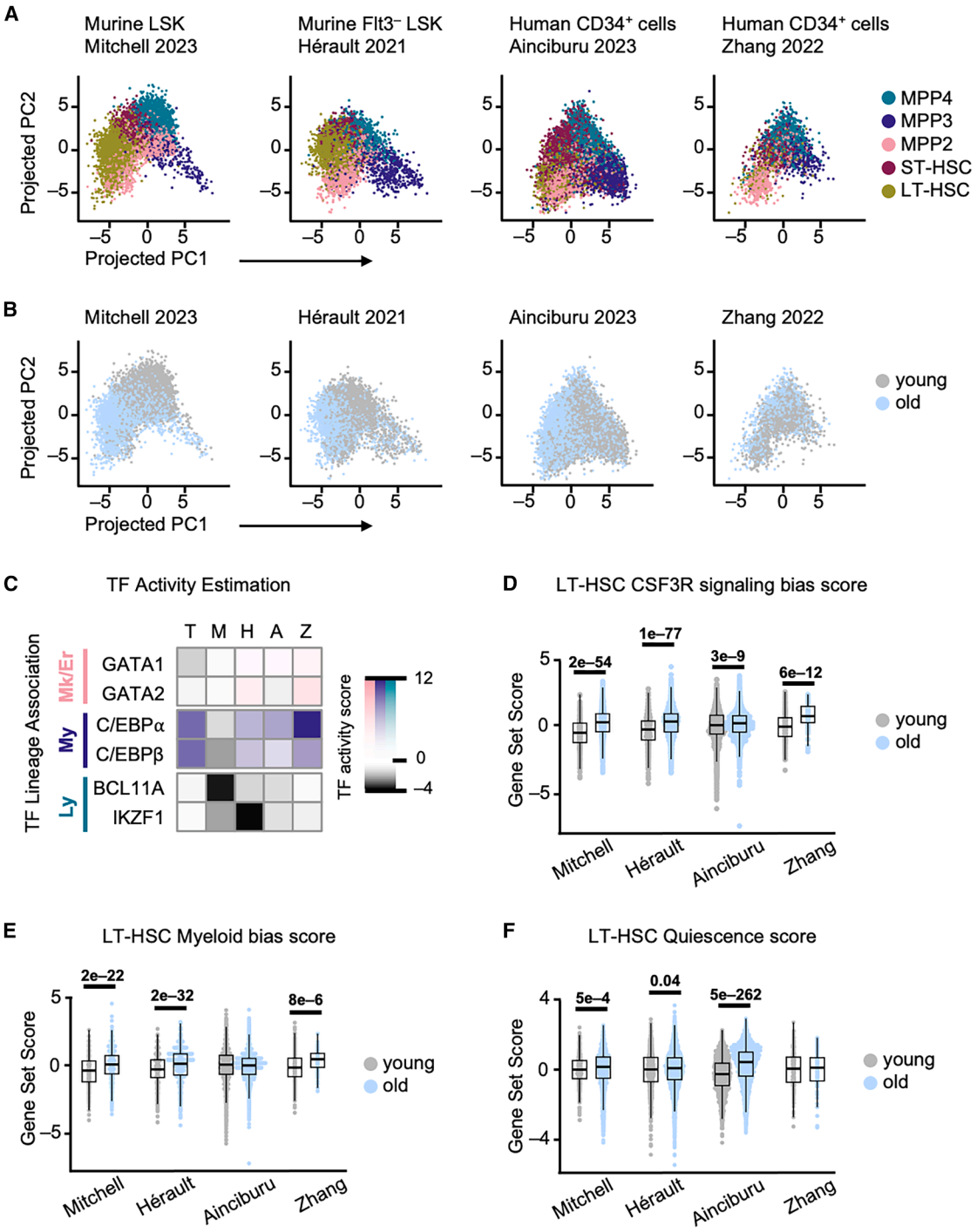

Figure 5. Aged HSCs from mice and humans show transcriptional myeloid bias and quiescence signatures

(A and B) scRNA-seq cells from previously published datasets projected onto PCA space from the transplant dataset, labeled by cell identity assignment (A) or age (B).

(C) TF activity estimation[46] in transplant (T), Mitchell et al.[41] (M), Hérault et al.[42] (H), Ainciburu et al.[43] (A), and Zhang et al.[44] (Z) datasets.

(D–F) CSF3R bias (CSF3R response-lymphoid-associated genes) (D), myeloid bias (myeloid-associated-lymphoid-associated) genes (E), and quiescence gene[49] set score (F) among LT-HSCs, *z* scored for each dataset. Wilcoxon rank-sum test *p* values.

See also Figure S6 and Table S1.

HSCs differ from myeloid-biased HSCs, performing DEG analysis between aged LT-HSCs with high quiescence scores (top 25th percentile, pooled among datasets to increase statistical power) and those with high myeloid bias scores. In aged quiescence^{high} vs. myeloid^{high} LT-HSCs, there was significant downregulation in terms of cell cycle and mitotic division, as expected (Table S2). The top upregulated GO terms were for cell signaling, migration, and morphogenesis, pointing to aging-associated cytoskeletal changes[53] (Table S3). Intriguingly, the GO immune response term was also significantly enriched (BH-adjusted $p = 1.9 \times 10^{-9}$). Thus, the aged HSC pool shows heterogeneity with distinct transcriptional programs of myeloid bias and quiescence.

HSC-intrinsic NF-κB activity correlates with quiescence but not myeloid bias

As NF-κB controls immune responses, we examined whether NF-κB-response genes are differentially expressed in highly quiescent vs. myeloid-biased HSCs. Indeed, NF-κB-response genes[54] were 3.1-fold more abundant among the upregulated DEGs from highly quiescent HSCs (Figure 6A). Further, single-cell NF-κB gene set enrichment scores using sets of 270 murine and 248 human NF-κB-responsive genes,[54] including *Nfkbia*, *Ccl5*, and *Il1b*, were increased in aged LT-HSCs vs. young controls (Figure 6B). Two orthogonal approaches demonstrated a relationship between NF-κB and quiescence scores in aged HSCs but found no relationship between NF-κB and myeloid bias scores, either by calculating Spearman correlation between single-cell scores (Figures 6C–6E) or by determining the percentage of overlap between high-scoring cells (Figure 6F). Notably, the positive correlation between NF-κB and quiescence was consistent regardless of HSC age (Figure 6E), suggesting a consistent biological relationship independent of aging, though both signatures are potentiated in HSCs from aged individuals.

We next evaluated the relationships between transcriptional myeloid bias, NF-κB activity, and quiescence in scRNA-seq data from our hematopoietic-extrinsic IκB^{-} transplantation studies. Intriguingly, IκB^{-}-recipient LT-HSCs showed unchanged NF-κB scores compared to controls (Figure 6G) despite their myeloid-biased transcriptomic and epigenomic states (Figures 3 and 4). This distinction underscores the separation of HSC-intrinsic NF-κB activity from milieu-directed myeloid bias. Furthermore, LT-HSCs from IκB^{-} recipients showed reduced quiescence scores (Figure 6G), consistent with the lack of HSC accumulation observed in these mice. Positive per-cell correlations between NF-κB and quiescence, but not between NF-κB and myeloid bias/CSF3R bias, were similar to those seen in young and aged HSCs (Figure 6E). These findings demonstrate that the transcriptional programs supporting NF-κB activity, myeloid bias, and quiescence are all increased in HSCs upon aging. However, on a per-cell basis, HSC-intrinsic expression of NF-κB target genes is associated with higher quiescence signatures but not myeloid bias. The per-cell relationships between these transcriptional programs are conserved in murine and human HSCs across the age span.

Hematopoietic-intrinsic NF-κB activity drives functional HSC impairment

In addition to the close transcriptional relationship between NF-κB activity and quiescence, we also observed that NF-κB RelA protein is more abundant in quiescent LT-HSCs vs. more proliferative ST-HSCs in mVenus-RelA reporter mice (Figures 1A and 1B). Quiescent G0 cells lack expression of the Ki67 antigen,[55] and we found that IκB^{-} LT-HSCs contain a higher proportion of Ki67-negative G0 cells than WT controls (Figure 7A). This increase in G0 proportion is not attributable to a concomitant increase in apoptosis, as Annexin V staining is reduced in IκB^{-} LT-HSCs compared to WT (Figure S7A). These results support the transcriptomic evidence of an association between NF-κB activity and HSC quiescence.

We then tested whether experimentally elevating NF-κB within HSCs impacts their functional reconstitution capacity using a transplantation approach. NF-κB activity alters *Cxcr4* expression (Figure 4C),[56] a critical chemokine for HSC homing; therefore, competitive transplantation between IκB^{-} and WT HSCs may show differences in niche homing and occupancy that could overshadow quiescence-mediated phenotypes. Thus, we performed IκB^{-} hematopoietic-intrinsic transplantation experiments in a non-competitive manner. Primary bone marrow transplantation of IκB^{-} donor cells into WT recipients revealed reduced engraftment compared to WT donor controls at 16 weeks (peripheral blood chimerism 94% in WT donors vs. 69% in IκB^{-} donors; bone marrow chimerism 99% in WT donors vs. 88% in IκB^{-} donors; Figures 7B, 7C, and S7B). Immunophenotyping confirmed that the reduction in circulating B cells in IκB^{-} mice is mediated through a hematopoietic-intrinsic mechanism (Figures S7C and S7D). Bone marrow cellularity did not differ between mice receiving WT- vs. IκB^{-} donor marrow; however, an increase in total HSPCs was noted in IκB^{-} donor marrow, driven by increases in MPP2s, MPP3s, and MPP4s and opposed by reduced ST-HSCs (Figures 7D and S7E). In contrast to non-transplanted IκB^{-} mice, LT-HSC numbers were significantly lower in IκB^{-} donor marrow vs. WT controls (Figure 7D). HSPCs and maturing hematopoietic cells can both release and respond to proinflammatory cytokines and other paracrine signals.[57] Thus, transplanted IκB^{-} hematopoietic cells and their mature progeny may secrete mediators that promote an inflammatory milieu and/or remodel their niches. Therefore, HSPC expansion and ST-HSC reduction common to both IκB^{-} hematopoietic-intrinsic transplants and non-transplanted IκB^{-} mice may be attributable to either hematopoietic-intrinsic effects or to responses to hematopoietic-derived inflammatory mediators. In contrast, the reduction in LT-HSC numbers, which is unique to IκB^{-} donor cell transplants and not seen in non-transplanted IκB^{-} mice, suggests that LT-HSC-autonomous NF-κB activity limits their expansion or maintenance and can be opposed by NF-κB activity in the non-hematopoietic compartment.

We further tested IκB^{-} HSC function by stressing their repopulation capacity upon secondary transplantation, resulting in a marked engraftment compromise of IκB^{-} donor cells compared to WT controls (peripheral blood chimerism 92% in WT donors vs. 39% in IκB^{-} donors; bone marrow chimerism 98% in WT donors vs. 54% in IκB^{-} donors; Figures 7E, 7F, S7F, and S7G). In addition, bone marrow cellularity and HSPC numbers were reduced (Figure 7G). Among HSPCs, LT-HSCs and ST-HSCs were both significantly reduced in number, and no lineage bias among MPP subsets nor bone marrow granulocytosis was observed (Figures 7G, S7H, and S7I). These

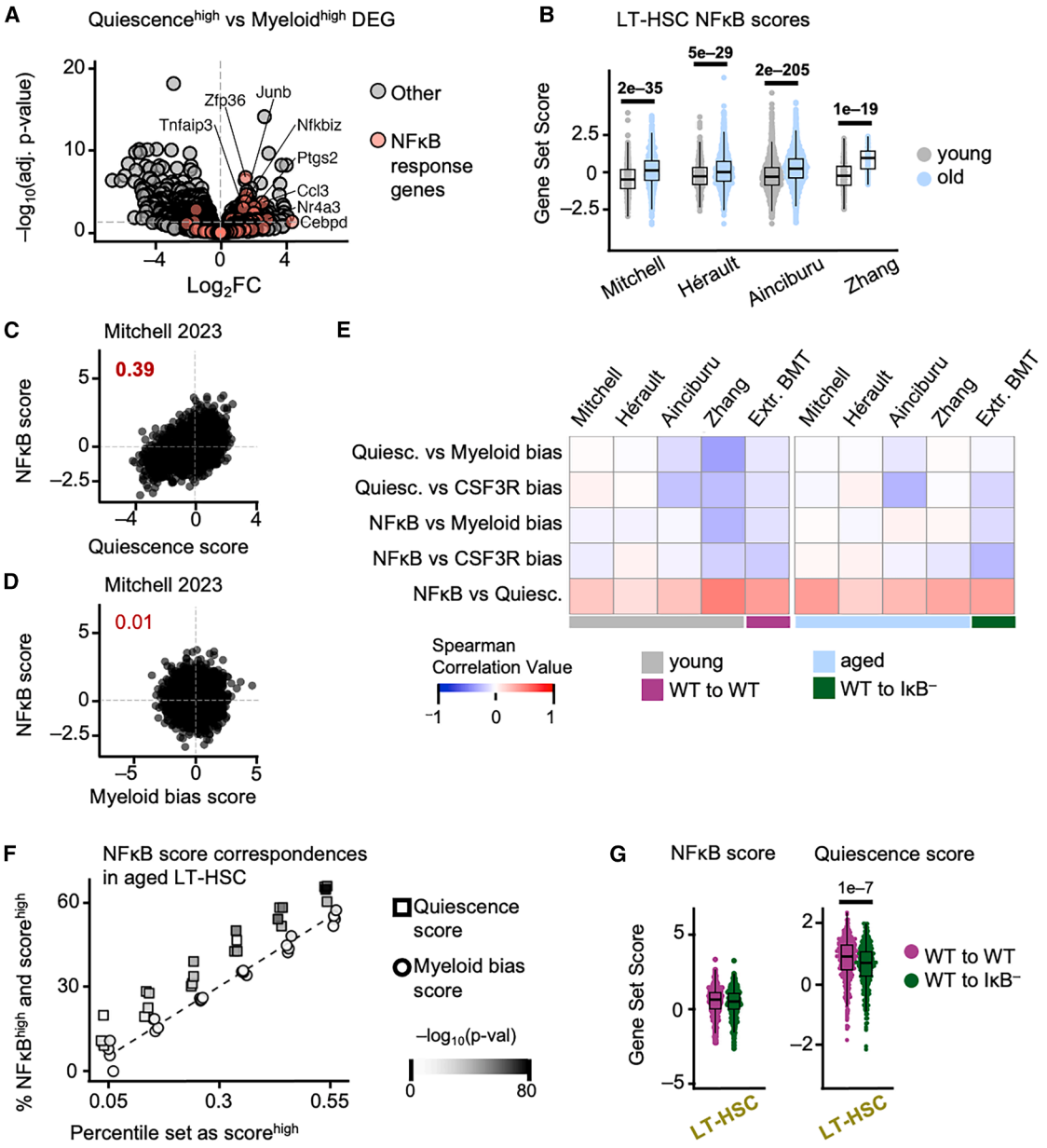

Figure 6. In HSCs, NF-κB signatures correlate with quiescence but not myeloid bias

(A) DEGs between cells in the top 25th percentile for quiescence score ("quiescence^{high}") vs. top 25th percentile for myeloid bias ("myeloid^{high}"), combined for all old LT-HSCs across datasets; BH-adjusted *p* values.

(B) NF-κB-response gene scores among LT-HSCs in aging datasets, *z* scored for each dataset.

(C) LT-HSC single-cell correspondence between quiescence and NF-κB-response gene set scores; inset: Spearman correlation value.

(D) LT-HSC single-cell correspondence between NF-κB-response gene and myeloid bias scores; inset: Spearman correlation value.

(E) Spearman correlations between single-cell gene scores for all datasets.

(F) For aged LT-HSCs at specific percentile thresholds (*x* axis), percentage of cells that reach both NF-κB^{high} and quiescence^{high} (square) or both NF-κB^{high} and myeloid^{high} (circle) thresholds; the dashed line indicates the expected values if no relationship between NF-κB score and the comparator score is observed.

(G) NF-κB-response and quiescence gene set scores among LT-HSCs from primary hematopoietic-extrinsic transplant dataset.

(B and G) Wilcoxon rank-sum test *p* values; bold typeface indicates an increase in the mean vs. control. See also Figure S6 and Tables S2 and S3.

findings demonstrate durable hematopoietic impairment 16 weeks following secondary transplantation. The lack of HSPC expansion or bone marrow myeloid bias upon secondary transplantation of IκB^{-} donor marrow further supports that hematopoietic-autonomous NF-κB activity is insufficient for durable myeloid bias. Together, these observations indicate that elevated hematopoietic-intrinsic NF-κB drives functional HSC impairment with reduced long-term bone marrow reconstitution

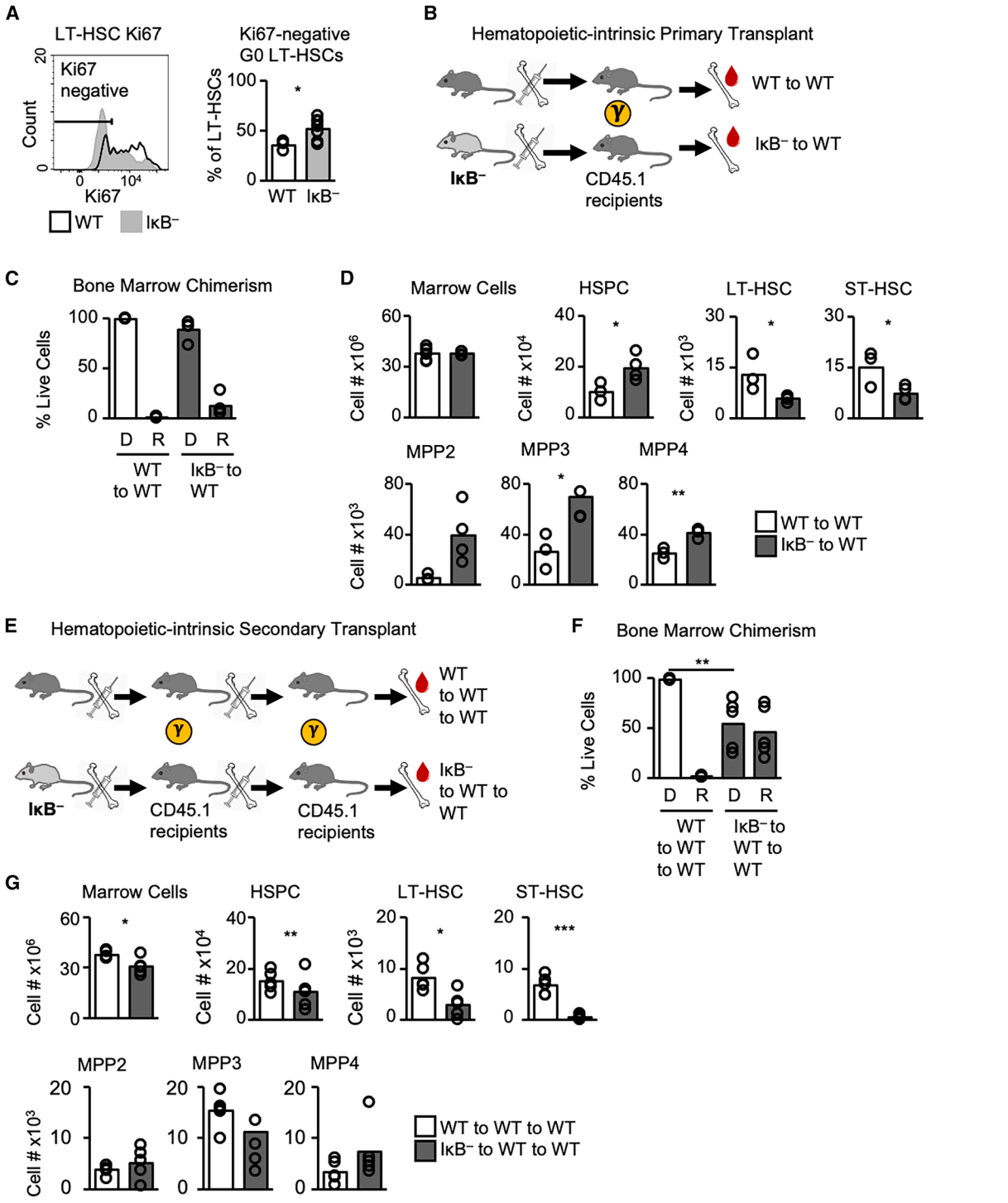

Figure 7. Experimentally elevated NF-κB activity within HSCs impairs bone marrow reconstitution capacity

(A) Representative Ki67 distribution in WT and IκB⁻ LT-HSCs (left) and quantification of Ki67-negative G0 LT-HSCs (right); *n* = 3–7.

(B) Primary transplant schematic.

(C) Bone marrow chimerism at 15 weeks. D, donor; R, recipient.

(D) Donor bone marrow, HSPC, and HSPC subset cell numbers.

(E) Secondary transplant schematic.

(legend continued on next page)

capacity and is mechanistically separable from progenitor myeloid bias.

DISCUSSION

By establishing the IκB^{-} model of elevated NF-κB activity, we enabled the identification of distinct roles of NF-κB in hematopoietic aging: in producing an inflammatory milieu that drives HSC epigenomic reprogramming and myeloid bias and within HSCs in promoting their quiescence and limiting functional bone marrow reconstitution. In contrast, HSC accumulation appears independent of NF-κB. These findings demonstrate that while myeloid bias and HSC dysfunction co-occur in aging, they are mechanistically separable and are coordinated by NF-κB in different cellular compartments.

A strength of the IκB^{-} model is its broad applicability to diverse states of inflammation. HSPCs, mature hematopoietic cells, and niche cells are all sources of inflammatory mediators in aging.[58,59] Chronic inflammation may originate systemically from the microbiota, in association with infection, cancer, autoimmune/inflammatory disease, and others.[60] Despite variation in the quality, strength, and cellular sources of inflammatory mediators between aging individuals, the phenotypes of myeloid bias, HSC dysfunction, and HSC accumulation are remarkably consistent. By targeting NF-κB, a central regulatory node that integrates acute and chronic inflammatory signals, the IκB^{-} mouse is a robust model with broad relevance. IκB^{-} mice display myeloid bias and HSC dysfunction similar to aged mice. In contrast, this model demonstrates that systemically elevated NF-κB activity is insufficient to drive the HSC accumulation seen in aging. Indeed, HSC pool size varies considerably between other models of systemic inflammation that display myeloid bias,[1] suggesting that HSC accumulation may require additional perturbations such as DNA damage, metabolic derangements, or others.[61] In future studies, models such as IκB^{-} may be useful to interrogate diverse chronic inflammatory states affecting HSCs beyond aging, such as myeloid neoplasia, bone marrow failure, iatrogenic immunomodulation, and more.[62,63]

NF-κB activity exerts different effects in different cell types,[6,8] and our findings clarify the functional pleiotropism of NF-κB in HSCs vs. their environments. Appreciating this diversity in NF-κB-mediated functions sheds new light on the seemingly contradictory effects attributed to several cytokines and growth factors on hematopoiesis. Tumor necrosis factor (TNF) is elevated in the bone marrow of both IκB^{-} and aged mice. Yet, TNF signaling (mediated through NF-κB) can restrict HSC proliferation/reconstitution and promote HSC expansion and myeloid bias.[64–66] Our findings raise the possibility that reduced bone marrow reconstitution capacity following acute TNF may be mediated by HSC-intrinsic responses, while myeloid bias following chronic TNF exposure may be mediated through the milieu. Interleukin (IL)-1 signaling is similarly appreciated to promote myeloid bias through a niche-mediated mechanism.[41] Colony-stimulating factors produced by the niche are NF-κB inducible, and an endothelial cell NF-κB-CSF3 axis is recognized in emergency myelopoiesis.[67,68] Concordantly, we found increased CSF3 in aged and IκB^{-}-recipient bone marrow and higher CSF3R transcriptional responses in aged and IκB^{-}-recipient HSCs. However, while niche-derived acute CSF3 in emergency myelopoiesis is a potent inducer of myeloid differentiation and HSC mobilization, chronic CSF3 signaling is instead associated with HSC-autonomous quiescence and functional decline in a TLR/MyD88-dependent manner.[69] TLR/MyD88 signaling is mediated in large part through NF-κB,[10] and thus, our findings may reconcile these apparently opposing effects of CSF3 signaling in acute vs. chronic settings. Thus, our findings delineating the pleiotropic roles of NF-κB signaling in HSCs and their environments clarify the complex roles of cytokines and growth factors in hematopoiesis.

In aging, inflammation and myeloid bias co-occur, leading to initial assumptions that these phenotypes were co-driven in a cell-intrinsic manner.[70] In support of this view, aged LT-HSCs harbor cell-autonomous transcriptional programs of myeloid bias and respond to inflammatory cues.[58,71–73] However, there is mounting evidence for myeloid bias mediated by the sympathetic nervous system, vascular networks, mesenchymal lineage cells, and others.[74–77] Our own recent work described milieu-directed myeloid bias in aging, IκB^{-} mice, and myeloid neoplasms that requires both differentiation bias and progenitor proliferation using mathematical models of early hematopoiesis.[78] Here, our studies demonstrate that an inflamed bone marrow milieu is sufficient for phenotypic, transcriptomic, and epigenomic myeloid bias of LT-HSCs. By identifying milieu-directed inflammation as a driver of HSC-intrinsic epigenomic and transcriptomic reprogramming, our findings reconcile the prior data in support of both HSC-extrinsic and HSC-autonomous mechanisms of myeloid bias.

HSC epigenomic programming directs the cell fates of their progeny.[79] We identified premature or inappropriate epigenomic and transcriptomic myeloid signatures in HSCs underlying milieu-directed myeloid bias. A cell labeling methodology enabled comparisons across omics modalities, datasets, and species to generate these insights. In an inflamed niche, HSCs showed increased C/EBP motif accessibility. This is consistent with a lipopolysaccharide (LPS)-induced inflammation model,[80] yet our findings further demonstrate that HSC epigenomic reprogramming is directed by an inflammatory milieu rather than via HSC-autonomous responses. Lineage-primed MPPs are immediate HSC progeny that can transdifferentiate, with phenotypic megakaryocyte/erythroid-primed MPP2s and lymphoid-primed MPP4s contributing to myeloid output in inflammatory and regenerative contexts.[18] We identified potentiated C/EBP and PU.1 TF accessibility in MPP4s, raising the possibility that HSC epigenomic reprogramming may be heritable and contribute to apparent MPP transdifferentiation. This would be in line with previous studies showing that C/EBP

(F) Bone marrow chimerism at 16 weeks.
(G) Donor bone marrow, HSPC, and HSPC subset cell numbers.
(B–D) $n = 3–4$, one transplant batch. (E–G) $n = 5$, one transplant batch. Unpaired Student's two-tailed t test p values. *$p < 0.05$, **$p < 0.01$, and ***$p < 0.001$. See also Figure S7.

ectopic overexpression and high PU.1 favor myeloid cell fates over lymphoid.[27] We establish that increased C/EBP activity occurs in a natural setting of MPP differentiation bias, clarifying that the previous overexpression data are physiologically relevant. Secondary hematopoietic-extrinsic transplantation experiments further show that phenotypic progenitor myeloid bias is reversible upon re-transplantation to a non-NF-κB-dysregulated milieu, despite HSC epigenomic reprogramming. While our work and that of others have shown reversibility of phenotypic myeloid bias,[72,80] it will be of interest in future studies to test the effect of long-term exposure to an inflamed milieu on the HSC epigenome and hematopoietic output. Our results support HSCs as an important reservoir of immunological memory that is modifiable by milieu-derived signals, further pointing to the bone marrow niche as a potential therapeutic target for disordered hematopoiesis.

We show that hematopoietic-intrinsic NF-κB activity is associated with stem cell quiescence and diminished bone marrow reconstitution, similar to aging and inflammatory challenges.[1,81] While paracrine mediators of HSC quiescence and maintenance are produced by local niches,[82] our findings raise the possibility of an additional HSC-intrinsic mechanism of quiescence regulation. Previously, NF-κB pathway activation via lymphotoxin β receptor (LTβR) agonism or IKK-activating mutations provided conflicting evidence regarding its impact on HSC quiescence.[83,84] However, unlike the IκB^{-} model, these prior models modulate pathways other than NF-κB, such as MAPK, autophagy, and others.[10,13] Here, we observed that HSC NF-κB activity and quiescence signatures are positively correlated across the age span, and both are potentiated in aging. IκB^{-} HSCs also showed a higher proportion of Ki67-negative G0 cells. These findings are compatible with the steady-state dependence of HSCs on NF-κB signaling[85] and the sensitivity of aged HSCs to elevated NF-κB signaling that limits their self-renewal.[86] Per-cell transcriptomic analyses reveal heterogeneity within the HSC pool, enabling new appreciation that transcriptional programs of myeloid bias are independent of HSC-intrinsic inflammatory NF-κB responses and further supporting the framework of milieu-directed myeloid bias.

Phenotypic HSC heterogeneity in the expression of CD150 separates CD150^{high} myHSCs that accumulate in aging from CD150^{low} lymphoid-biased HSCs (lyHSCs).[22] While IκB^{-} mice showed no difference in myHSC vs. lyHSC abundances, Semaphorin 4A mediates HSC inflammatory stress in a non-cell-autonomous manner.[87] Thus, non-NF-κB-driven mechanisms may control myHSC vs. lyHSC phenotype specification. As myHSCs have been proposed as a target to improve suppressed lymphoid development and viral responses in aging,[72] further work examining the regulation of HSC heterogeneity in steady-state, aging, and stress conditions will be important.

Our findings establish that inflammation-driven myeloid bias and HSC dysfunction are separable phenomena and raise the possibility that distinct NF-κB functions within HSCs and their cellular milieu may balance niche-derived emergency hematopoietic signals with HSC-driven quiescence and preservation. This suggests that HSCs and their environments should be considered independently when developing therapeutic strategies to improve hematopoiesis in the setting of immune dysregulation.

Limitations of the study

Here, we show that NF-κB responses in hematopoietic cells vs. in their milieu drive different aspects of hematopoietic aging. Some limitations are noted. First, irradiation of recipient mice for transplantation induces inflammation, which may have diminished the sensitivity of detecting mutant-specific effects. Second, these studies do not delineate the contribution of different milieu cell types, which will require new mouse models and may be the goal of future studies. Third, NF-κB-driven HSC dysfunction, including increased quiescence, is challenging to functionally assess, as the transcriptomic hallmarks are detected using destructive sequencing assays. Limiting-dilution HSC transplantation experiments may be useful in future studies.

RESOURCE AVAILABILITY

Lead contact

Requests for further information and resources should be directed to and will be fulfilled by the lead contact, Alexander Hoffmann (ahoffmann@ucla.edu).

Materials availability

Mouse lines generated in this study are available from the lead contact without restriction.

Data and code availability

- scRNA-seq and ATAC-seq data generated in this study are available at GEO under accession numbers GEO: GSE261946 and GEO: GSE264569 and are publicly available as of the date of publication.
- Original code and processed data objects have been deposited at Zenodo: https://doi.org/10.5281/zenodo.10828398. They are publicly available as of the date of publication.
- Any additional information required to reanalyze the data reported in this paper is available from the lead contact upon request.

ACKNOWLEDGMENTS

The authors thank Kylie Farrell and the UCLA JCCC, BSCRC, TCGB, IAC, and TPCL core facilities for technical assistance and Quen Cheng for feedback on the manuscript. This research was funded by NIH R01CA264986 to D.S.R. and NIH R01AI127867, R01AI173214, and R01AI132731 to A.H. J.J.C. acknowledges support from the California Institute for Regenerative Medicine Broad Stem Cell Research Training Program, and A.S. acknowledges support from NIH T32GM008185 and T32GM008042.

AUTHOR CONTRIBUTIONS

Conceptualization, J.J.C. and A.H.; methodology, J.J.C., A.S., Y.-S.L., Y.L., and J.K.K.; investigation, J.J.C., Y.-S.L., Y.L., T.T., and J.K.K.; formal analysis, J.J.C., A.S., N.P., and D.M.; resources, D.S.R. and A.H.; writing, J.J.C. and A.H.; supervision, D.S.R. and A.H.; funding acquisition, D.S.R. and A.H.

DECLARATION OF INTERESTS

D.S.R. has served as a consultant to AbbVie, a pharmaceutical company that develops and markets drugs for hematologic disorders. Y.L. contributed to this work prior to becoming an employee and shareholder at DeepKinase.

STAR★METHODS

Detailed methods are provided in the online version of this paper and include the following:

- KEY RESOURCES TABLE
- METHOD DETAILS
  - Mice

SUPPLEMENTAL INFORMATION

Supplemental information can be found online at https://doi.org/10.1016/j.celrep.2025.116193.

Received: February 20, 2025
Revised: June 12, 2025
Accepted: August 1, 2025
Published: August 26, 2025

REFERENCES

1. Caiado, F., Pietras, E.M., and Manz, M.G. (2021). Inflammation as a regulator of hematopoietic stem cell function in disease, aging, and clonal selection. J. Exp. Med. *218*, e20201541. https://doi.org/10.1084/jem.20201541.
2. Mejia-Ramirez, E., and Florian, M.C. (2020). Understanding intrinsic hematopoietic stem cell aging. Haematologica *105*, 22–37. https://doi.org/10.3324/haematol.2018.211342.
3. Urbán, N., and Cheung, T.H. (2021). Stem cell quiescence: the challenging path to activation. Development *148*, dev165084. https://doi.org/10.1242/dev.165084.
4. Tümpel, S., and Rudolph, K.L. (2019). Quiescence: Good and Bad of Stem Cell Aging. Trends Cell Biol. *29*, 672–685. https://doi.org/10.1016/j.tcb.2019.05.002.
5. Li, J., Malouf, C., Miles, L.A., Willis, M.B., Pietras, E.M., and King, K.Y. (2023). Chronic inflammation can transform the fate of normal and mutant hematopoietic stem cells. Exp. Hematol. *127*, 8–13. https://doi.org/10.1016/j.exphem.2023.08.008.
6. Hayden, M.S., West, A.P., and Ghosh, S. (2006). NF-κB and the immune response. Oncogene *25*, 6758–6780. https://doi.org/10.1038/sj.onc.1209943.
7. Kaltschmidt, C., Greiner, J.F.W., and Kaltschmidt, B. (2021). The Transcription Factor NF-κB in Stem Cells and Development. Cells *10*, 2042. https://doi.org/10.3390/cells10082042.
8. Rodriguez, B.N., Huang, H., Chia, J.J., and Hoffmann, A. (2024). The noncanonical NFκB pathway: Regulatory mechanisms in health and disease. WIREs Mechanisms of Disease *16*, e1646. https://doi.org/10.1002/wsbm.1646.
9. Chambers, S.M., Shaw, C.A., Gatza, C., Fisk, C.J., Donehower, L.A., and Goodell, M.A. (2007). Aging hematopoietic stem cells decline in function and exhibit epigenetic dysregulation. PLoS Biol. *5*, e201. https://doi.org/10.1371/journal.pbio.0050201.
10. Oeckinghaus, A., Hayden, M.S., and Ghosh, S. (2011). Crosstalk in NF-κB signaling pathways. Nat. Immunol. *12*, 695–708. https://doi.org/10.1038/ni.2065.
11. Mitroulis, I., Kalafati, L., Bornhäuser, M., Hajishengallis, G., and Chavakis, T. (2020). Regulation of the Bone Marrow Niche by Inflammation. Front. Immunol. *11*, 1540. https://doi.org/10.3389/fimmu.2020.01540.
12. García-García, V.A., Alameda, J.P., Page, A., and Casanova, M.L. (2021). Role of NF-κB in Ageing and Age-Related Diseases: Lessons from Genetically Modified Mouse Models. Cells *10*, 1906. https://doi.org/10.3390/cells10081906.
13. Schröfelbauer, B., and Hoffmann, A. (2011). How do pleiotropic kinase hubs mediate specific signaling by TNFR superfamily members? Immunol. Rev. *244*, 29–43. https://doi.org/10.1111/j.1600-065X.2011.01060.x.
14. Cheng, C.S., Feldman, K.E., Lee, J., Verma, S., Huang, D.-B., Huynh, K., Chang, M., Ponomarenko, J.V., Sun, S.-C., Benedict, C.A., et al. (2011). The specificity of innate immune responses is enforced by repression of interferon response elements by NF-κB p50. Sci. Signal. *4*, ra11. https://doi.org/10.1126/scisignal.2001501.
15. Navarro, H.I., Liu, Y., Fraser, A., Lefaudeux, D., Chia, J.J., Vong, L., Roifman, C.M., and Hoffmann, A. (2023). RelB-deficient autoinflammatory pathology presents as interferonopathy, but in mice is IFN-independent. J. Allergy Clin. Immunol. *152*, 1261–1272. https://doi.org/10.1016/j.jaci.2023.06.024.
16. Beg, A.A., Sha, W.C., Bronson, R.T., and Baltimore, D. (1995). Constitutive NF-kappa B activation, enhanced granulopoiesis, and neonatal lethality in I kappa B alpha-deficient mice. Genes Dev. *9*, 2736–2746. https://doi.org/10.1101/gad.9.22.2736.
17. Adelaja, A., Taylor, B., Sheu, K.M., Liu, Y., Luecke, S., and Hoffmann, A. (2021). Six distinct NFκB signaling codons convey discrete information to distinguish stimuli and enable appropriate macrophage responses. Immunity *54*, 916–930.e7. https://doi.org/10.1016/j.immuni.2021.04.011.
18. Pietras, E.M., Reynaud, D., Kang, Y.-A., Carlin, D., Calero-Nieto, F.J., Leavitt, A.D., Stuart, J.M., Göttgens, B., and Passegué, E. (2015). Functionally distinct subsets of lineage-biased multipotent progenitors control blood production in normal and regenerative conditions. Cell Stem Cell *17*, 35–46. https://doi.org/10.1016/j.stem.2015.05.003.
19. Yamamoto, R., Wilkinson, A.C., and Nakauchi, H. (2018). Changing concepts in hematopoietic stem cells. Science *362*, 895–896. https://doi.org/10.1126/science.aat7873.
20. Rao, P., Hayden, M.S., Long, M., Scott, M.L., West, A.P., Zhang, D., Oeckinghaus, A., Lynch, C., Hoffmann, A., Baltimore, D., and Ghosh, S. (2010). IkappaBbeta acts to inhibit and activate gene expression during the inflammatory response. Nature *466*, 1115–1119. https://doi.org/10.1038/nature09283.
21. Hoffmann, A., Levchenko, A., Scott, M.L., and Baltimore, D. (2002). The IkappaB-NF-kappaB signaling module: temporal control and selective gene activation. Science *298*, 1241–1245. https://doi.org/10.1126/science.1071914.
22. Beerman, I., Bhattacharya, D., Zandi, S., Sigvardsson, M., Weissman, I.L., Bryder, D., and Rossi, D.J. (2010). Functionally distinct hematopoietic stem cells modulate hematopoietic lineage potential during aging by a mechanism of clonal expansion. Proc. Natl. Acad. Sci. USA *107*, 5465–5470. https://doi.org/10.1073/pnas.1000834107.
23. Busch, K., and Rodewald, H.-R. (2016). Unperturbed vs. post-transplantation hematopoiesis: both in vivo but different. Curr. Opin. Hematol. *23*, 295–303. https://doi.org/10.1097/MOH.0000000000000250.
24. Nishi, K., Sakamaki, T., Sadaoka, K., Fujii, M., Takaori-Kondo, A., Chen, J.Y., and Miyanishi, M. (2022). Identification of the minimum requirements for successful haematopoietic stem cell transplantation. Br. J. Haematol. *196*, 711–723. https://doi.org/10.1111/bjh.17867.
25. Peled, A., Gonzalo, J.A., Lloyd, C., and Gutierrez-Ramos, J.C. (1998). The chemotactic cytokine eotaxin acts as a granulocyte-macrophage colony-stimulating factor during lung inflammation. Blood *91*, 1909–1916.
26. Katsumura, K.R., and Bresnick, E.H.; GATA Factor Mechanisms Group (2017). The GATA factor revolution in hematology. Blood *129*, 2092–2102. https://doi.org/10.1182/blood-2016-09-687871.
27. Tsukada, J., Yoshida, Y., Kominato, Y., and Auron, P.E. (2011). The CCAAT/enhancer (C/EBP) family of basic-leucine zipper (bZIP) transcription factors is a multifaceted highly-regulated system for gene regulation. Cytokine *54*, 6–19. https://doi.org/10.1016/j.cyto.2010.12.019.
28. Bouderlique, T., Peña-Pérez, L., Kharazi, S., Hils, M., Li, X., Krstic, A., De Paepe, A., Schachtrup, C., Gustafsson, C., Holmberg, D., et al. (2019). The Concerted Action of E2-2 and HEB Is Critical for Early Lymphoid

Specification. Front. Immunol. *10*, 455. https://doi.org/10.3389/fimmu.2019.00455.

29. Fric, J., Lim, C.X.F., Koh, E.G.L., Hofmann, B., Chen, J., Tay, H.S., Mohammad Isa, S.A.B., Mortellaro, A., Ruedl, C., and Ricciardi-Castagnoli, P. (2012). Calcineurin/NFAT signalling inhibits myeloid haematopoiesis. EMBO Mol. Med. *4*, 269–282. https://doi.org/10.1002/emmm.201100207.

30. Higa, K.C., Goodspeed, A., Chavez, J.S., De Dominici, M., Danis, E., Zaberezhnyy, V., Rabe, J.L., Tenen, D.G., Pietras, E.M., and DeGregori, J. (2021). Chronic interleukin-1 exposure triggers selection for Cebpa-knockout multipotent hematopoietic progenitors. J. Exp. Med. *218*, e20200560. https://doi.org/10.1084/jem.20200560.

31. Laslo, P., Pongubala, J.M.R., Lancki, D.W., and Singh, H. (2008). Gene regulatory networks directing myeloid and lymphoid cell fates within the immune system. Semin. Immunol. *20*, 228–235. https://doi.org/10.1016/j.smim.2008.08.003.

32. Frederick, M.A., Williamson, K.E., Fernandez Garcia, M., Ferretti, M.B., McCarthy, R.L., Donahue, G., Luzete Monteiro, E., Takenaka, N., Reynaga, J., Kadoch, C., and Zaret, K.S. (2023). A pioneer factor locally opens compacted chromatin to enable targeted ATP-dependent nucleosome remodeling. Nat. Struct. Mol. Biol. *30*, 31–37. https://doi.org/10.1038/s41594-022-00886-5.

33. Jakobsen, J.S., Bagger, F.O., Hasemann, M.S., Schuster, M.B., Frank, A.-K., Waage, J., Vitting-Seerup, K., and Porse, B.T. (2015). Amplification of pico-scale DNA mediated by bacterial carrier DNA for small-cell-number transcription factor ChIP-seq. BMC Genom. *16*, 46. https://doi.org/10.1186/s12864-014-1195-4.

34. Link, V.M., Duttke, S.H., Chun, H.B., Holtman, I.R., Westin, E., Hoeksema, M.A., Abe, Y., Skola, D., Romanoski, C.E., Tao, J., et al. (2018). Analysis of Genetically Diverse Macrophages Reveals Local and Domain-wide Mechanisms that Control Transcription Factor Binding and Function. Cell *173*, 1796–1809.e17. https://doi.org/10.1016/j.cell.2018.04.018.

35. Comoglio, F., Simonatto, M., Polletti, S., Liu, X., Smale, S.T., Barozzi, I., and Natoli, G. (2019). Dissection of acute stimulus-inducible nucleosome remodeling in mammalian cells. Genes Dev. *33*, 1159–1174. https://doi.org/10.1101/gad.326348.119.

36. Rodriguez-Fraticelli, A.E., Wolock, S.L., Weinreb, C.S., Panero, R., Patel, S.H., Jankovic, M., Sun, J., Calogero, R.A., Klein, A.M., and Camargo, F.D. (2018). Clonal analysis of lineage fate in native haematopoiesis. Nature *553*, 212–216. https://doi.org/10.1038/nature25168.

37. Foroutan, M., Bhuva, D.D., Lyu, R., Horan, K., Cursons, J., and Davis, M.J. (2018). Single sample scoring of molecular phenotypes. BMC Bioinf. *19*, 404. https://doi.org/10.1186/s12859-018-2435-4.

38. Kwok, I., Becht, E., Xia, Y., Ng, M., Teh, Y.C., Tan, L., Evrard, M., Li, J.L.Y., Tran, H.T.N., Tan, Y., et al. (2020). Combinatorial Single-Cell Analyses of Granulocyte-Monocyte Progenitor Heterogeneity Reveals an Early Uni-potent Neutrophil Progenitor. Immunity *53*, 303–318.e5. https://doi.org/10.1016/j.immuni.2020.06.005.

39. Jiang, P., Zhang, Y., Ru, B., Yang, Y., Vu, T., Paul, R., Mirza, A., Altan-Bonnet, G., Liu, L., Ruppin, E., et al. (2021). Systematic investigation of cytokine signaling activity at the tissue and single-cell levels. Nat. Methods *18*, 1181–1191. https://doi.org/10.1038/s41592-021-01274-5.

40. Rothenberg, E.V. (2021). Single-cell insights into the hematopoietic generation of T-lymphocyte precursors in mouse and human. Exp. Hematol. *95*, 1–12. https://doi.org/10.1016/j.exphem.2020.12.005.

41. Mitchell, C.A., Verovskaya, E.V., Calero-Nieto, F.J., Olson, O.C., Swann, J.W., Wang, X., Hérault, A., Dellorusso, P.V., Zhang, S.Y., Svendsen, A.F., et al. (2023). Stromal niche inflammation mediated by IL-1 signalling is a targetable driver of haematopoietic ageing. Nat. Cell Biol. *25*, 30–41. https://doi.org/10.1038/s41556-022-01053-0.

42. Hérault, L., Poplineau, M., Mazuel, A., Platet, N., Remy, É., and Duprez, E. (2021). Single-cell RNA-seq reveals a concomitant delay in differentiation and cell cycle of aged hematopoietic stem cells. BMC Biol. *19*, 19. https://doi.org/10.1186/s12915-021-00955-z.

43. Ainciburu, M., Ezponda, T., Berastegui, N., Alfonso-Pierola, A., Vilas-Zornoza, A., San Martin-Uriz, P., Alignani, D., Lamo-Espinosa, J., San-Julian, M., Jiménez-Solas, T., et al. (2023). Uncovering perturbations in human hematopoiesis associated with healthy aging and myeloid malignancies at single-cell resolution. eLife *12*, e79363. https://doi.org/10.7554/eLife.79363.

44. Zhang, Y., Xie, X., Huang, Y., Liu, M., Li, Q., Luo, J., He, Y., Yin, X., Ma, S., Cao, W., et al. (2022). Temporal molecular program of human hematopoietic stem and progenitor cells after birth. Dev. Cell *57*, 2745–2760.e6. https://doi.org/10.1016/j.devcel.2022.11.013.

45. Gao, S., Wu, Z., Kannan, J., Mathews, L., Feng, X., Kajigaya, S., and Young, N.S. (2021). Comparative Transcriptomic Analysis of the Hematopoietic System between Human and Mouse by Single Cell RNA Sequencing. Cells *10*, 973. https://doi.org/10.3390/cells10050973.

46. Badia-i-Mompel, P., Vélez Santiago, J., Braunger, J., Geiss, C., Dimitrov, D., Müller-Dott, S., Taus, P., Dugourd, A., Holland, C.H., Ramirez Flores, R.O., and Saez-Rodriguez, J. (2022). decoupleR: ensemble of computational methods to infer biological activities from omics data. Bioinform. Adv. *2*, vbac016. https://doi.org/10.1093/bioadv/vbac016.

47. Laurenti, E., Doulatov, S., Zandi, S., Plumb, I., Chen, J., April, C., Fan, J.-B., and Dick, J.E. (2013). The transcriptional architecture of early human hematopoiesis identifies multilevel control of lymphoid commitment. Nat. Immunol. *14*, 756–763. https://doi.org/10.1038/ni.2615.

48. Heizmann, B., Kastner, P., and Chan, S. (2018). The Ikaros family in lymphocyte development. Curr. Opin. Immunol. *51*, 14–23. https://doi.org/10.1016/j.coi.2017.11.005.

49. Cheung, T.H., and Rando, T.A. (2013). Molecular regulation of stem cell quiescence. Nat. Rev. Mol. Cell Biol. *14*, 329–340. https://doi.org/10.1038/nrm3591.

50. van Velthoven, C.T.J., and Rando, T.A. (2019). Stem Cell Quiescence: Dynamism, Restraint, and Cellular Idling. Cell Stem Cell *24*, 213–225. https://doi.org/10.1016/j.stem.2019.01.001.

51. Singh, S., Jakubison, B., and Keller, J.R. (2020). Protection of hematopoietic stem cells from stress-induced exhaustion and aging. Curr. Opin. Hematol. *27*, 225–231. https://doi.org/10.1097/MOH.0000000000000586.

52. Yang, L., Wang, L., Geiger, H., Cancelas, J.A., Mo, J., and Zheng, Y. (2007). Rho GTPase Cdc42 coordinates hematopoietic stem cell quiescence and niche interaction in the bone marrow. Proc. Natl. Acad. Sci. USA *104*, 5091–5096. https://doi.org/10.1073/pnas.0610819104.

53. Higuchi-Sanabria, R., Paul, J.W., Durieux, J., Benitez, C., Frankino, P.A., Tronnes, S.U., Garcia, G., Daniele, J.R., Monshietehadi, S., and Dillin, A. (2018). Spatial regulation of the actin cytoskeleton by HSF-1 during aging. Mol. Biol. Cell *29*, 2522–2527. https://doi.org/10.1091/mbc.E18-06-0362.

54. Sheu, K.M., Guru, A.A., and Hoffmann, A. (2023). Quantifying stimulus-response specificity to probe the functional state of macrophages. Cell Syst. *14*, 180–195.e5. https://doi.org/10.1016/j.cels.2022.12.012.

55. Gerdes, J., Lemke, H., Baisch, H., Wacker, H.H., Schwab, U., and Stein, H. (1984). Cell cycle analysis of a cell proliferation-associated human nuclear antigen defined by the monoclonal antibody Ki-67. J. Immunol. *133*, 1710–1715.

56. Helbig, G., Christopherson, K.W., Bhat-Nakshatri, P., Kumar, S., Kishimoto, H., Miller, K.D., Broxmeyer, H.E., and Nakshatri, H. (2003). NF-kappaB promotes breast cancer cell migration and metastasis by inducing the expression of the chemokine receptor CXCR4. J. Biol. Chem. *278*, 21631–21638. https://doi.org/10.1074/jbc.M300609200.

57. Chavakis, T., Mitroulis, I., and Hajishengallis, G. (2019). Hematopoietic progenitor cells as integrative hubs for adaptation to and fine-tuning of inflammation. Nat. Immunol. *20*, 802–811. https://doi.org/10.1038/s41590-019-0402-5.

58. Zhao, J.L., Ma, C., O'Connell, R.M., Mehta, A., Diloreto, R., Heath, J.R., and Baltimore, D. (2014). Conversion of danger signals into cytokine signals by hematopoietic stem and progenitor cells for regulation of stress-induced hematopoiesis. Cell Stem Cell *14*, 445–459. https://doi.org/10.1016/j.stem.2014.01.007.

59. Helbling, P.M., Piñeiro-Yáñez, E., Gerosa, R., Boettcher, S., Al-Shahrour, F., Manz, M.G., and Nombela-Arrieta, C. (2019). Global Transcriptomic Profiling of the Bone Marrow Stromal Microenvironment during Postnatal Development, Aging, and Inflammation. Cell Rep. *29*, 3313–3330.e4. https://doi.org/10.1016/j.celrep.2019.11.004.

60. Hormaechea-Agulla, D., Le, D.T., and King, K.Y. (2020). Common Sources of Inflammation and Their Impact on Hematopoietic Stem Cell Biology. Curr. Stem Cell Rep. *6*, 96–107. https://doi.org/10.1007/s40778-020-00177-z.

61. López-Otín, C., Blasco, M.A., Partridge, L., Serrano, M., and Kroemer, G. (2023). Hallmarks of aging: An expanding universe. Cell *186*, 243–278. https://doi.org/10.1016/j.cell.2022.11.001.

62. Craver, B.M., El Alaoui, K., Scherber, R.M., and Fleischman, A.G. (2018). The Critical Role of Inflammation in the Pathogenesis and Progression of Myeloid Malignancies. Cancers (Basel) *10*, 104. https://doi.org/10.3390/cancers10040104.

63. Wang, J., Erlacher, M., and Fernandez-Orth, J. (2022). The role of inflammation in hematopoiesis and bone marrow failure: What can we learn from mouse models? Front. Immunol. *13*, 951937. https://doi.org/10.3389/fimmu.2022.951937.

64. Yamashita, M., and Passegué, E. (2019). TNF-α Coordinates Hematopoietic Stem Cell Survival and Myeloid Regeneration. Cell Stem Cell *25*, 357–372.e7. https://doi.org/10.1016/j.stem.2019.05.019.

65. Pronk, C.J.H., Veiby, O.P., Bryder, D., and Jacobsen, S.E.W. (2011). Tumor necrosis factor restricts hematopoietic stem cell activity in mice: involvement of two distinct receptors. J. Exp. Med. *208*, 1563–1570. https://doi.org/10.1084/jem.20110752.

66. Etzrodt, M., Ahmed, N., Hoppe, P.S., Loeffler, D., Skylaki, S., Hilsenbeck, O., Kokkaliaris, K.D., Kaltenbach, H.-M., Stelling, J., Nerlov, C., and Schroeder, T. (2019). Inflammatory signals directly instruct PU.1 in HSCs via TNF. Blood *133*, 816–819. https://doi.org/10.1182/blood-2018-02-832998.

67. Boettcher, S., Gerosa, R.C., Radpour, R., Bauer, J., Ampenberger, F., Heikenwalder, M., Kopf, M., and Manz, M.G. (2014). Endothelial cells translate pathogen signals into G-CSF-driven emergency granulopoiesis. Blood *124*, 1393–1403. https://doi.org/10.1182/blood-2014-04-570762.

68. Poulos, M.G., Ramalingam, P., Gutkin, M.C., Kleppe, M., Ginsberg, M., Crowley, M.J.P., Elemento, O., Levine, R.L., Rafii, S., Kitajewski, J., et al. (2016). Endothelial-specific inhibition of NF-κB enhances functional haematopoiesis. Nat. Commun. *7*, 13829. https://doi.org/10.1038/ncomms13829.

69. Schuettpelz, L.G., Borgerding, J.N., Christopher, M.J., Gopalan, P.K., Romine, M.P., Herman, A.C., Woloszynek, J.R., Greenbaum, A.M., and Link, D.C. (2014). G-CSF regulates hematopoietic stem cell activity, in part, through activation of Toll-like receptor signaling. Leukemia *28*, 1851–1860. https://doi.org/10.1038/leu.2014.68.

70. Dorshkind, K., Höfer, T., Montecino-Rodriguez, E., Pioli, P.D., and Rodewald, H.-R. (2020). Do haematopoietic stem cells age? Nat. Rev. Immunol. *20*, 196–202. https://doi.org/10.1038/s41577-019-0236-2.

71. Mann, M., Mehta, A., de Boer, C.G., Kowalczyk, M.S., Lee, K., Haldeman, P., Rogel, N., Knecht, A.R., Farouq, D., Regev, A., and Baltimore, D. (2018). Heterogeneous Responses of Hematopoietic Stem Cells to Inflammatory Stimuli Are Altered with Age. Cell Rep. *25*, 2992–3005.e5. https://doi.org/10.1016/j.celrep.2018.11.056.

72. Ross, J.B., Myers, L.M., Noh, J.J., Collins, M.M., Carmody, A.B., Messer, R.J., Dhuey, E., Hasenkrug, K.J., and Weissman, I.L. (2024). Depleting myeloid-biased haematopoietic stem cells rejuvenates aged immunity. Nature *628*, 162–170. https://doi.org/10.1038/s41586-024-07238-x.

73. Rossi, D.J., Bryder, D., Zahn, J.M., Ahlenius, H., Sonu, R., Wagers, A.J., and Weissman, I.L. (2005). Cell intrinsic alterations underlie hematopoietic stem cell aging. Proc. Natl. Acad. Sci. USA *102*, 9194–9199. https://doi.org/10.1073/pnas.0503280102.

74. Schneider, R.K., Mullally, A., Dugourd, A., Peisker, F., Hoogenboezem, R., Van Strien, P.M.H., Bindels, E.M., Heckl, D., Büsche, G., Fleck, D., et al. (2017). Gli1 + Mesenchymal Stromal Cells Are a Key Driver of Bone Marrow Fibrosis and an Important Cellular Therapeutic Target. Cell Stem Cell *20*, 785–800.e8. https://doi.org/10.1016/j.stem.2017.03.008.

75. Ho, Y.H., del Toro, R., Rivera-Torres, J., Rak, J., Korn, C., García-García, A., Macías, D., González-Gómez, C., del Monte, A., Wittner, M., et al. (2019). Remodeling of Bone Marrow Hematopoietic Stem Cell Niches Promotes Myeloid Cell Expansion during Premature or Physiological. Cell Stem Cell *25*, 407–418.e6. https://doi.org/10.1016/j.stem.2019.06.007.

76. Maryanovich, M., Zahalka, A.H., Pierce, H., Pinho, S., Nakahara, F., Asada, N., Wei, Q., Wang, X., Ciero, P., Xu, J., et al. (2018). Adrenergic nerve degeneration in bone marrow drives aging of the hematopoietic stem cell niche. Nat. Med. *24*, 782–791. https://doi.org/10.1038/s41591-018-0030-x.

77. Raaijmakers, M.H.G.P., Mukherjee, S., Guo, S., Zhang, S., Kobayashi, T., Schoonmaker, J.A., Ebert, B.L., Al-Shahrour, F., Hasserjian, R.P., Scadden, E.O., et al. (2010). Bone progenitor dysfunction induces myelodysplasia and secondary leukaemia. Nature *464*, 852–857. https://doi.org/10.1038/nature08851.

78. Singh, A., Chia, J.J., Rao, D.S., and Hoffmann, A. (2025). Population dynamics modeling reveals myeloid bias involves both HSC differentiation and progenitor proliferation biases. Blood *145*, 1293–1308. https://doi.org/10.1182/blood.2024025598.

79. Meng, Y., Carrelha, J., Drissen, R., Ren, X., Zhang, B., Gambardella, A., Valletta, S., Thongjuea, S., Jacobsen, S.E., and Nerlov, C. (2023). Epigenetic programming defines haematopoietic stem cell fate restriction. Nat. Cell Biol. *25*, 812–822. https://doi.org/10.1038/s41556-023-01137-5.

80. de Laval, B., Maurizio, J., Kandalla, P.K., Brisou, G., Simonnet, L., Huber, C., Gimenez, G., Matcovitch-Natan, O., Reinhardt, S., David, E., et al. (2020). C/EBPβ-Dependent Epigenetic Memory Induces Trained Immunity in Hematopoietic Stem Cells. Cell Stem Cell *26*, 657–674.e8. https://doi.org/10.1016/j.stem.2020.01.017.

81. Bogeska, R., Mikecin, A.-M., Kaschutnig, P., Fawaz, M., Büchler-Schäff, M., Le, D., Ganuza, M., Vollmer, A., Paffenholz, S.V., Asada, N., et al. (2022). Inflammatory exposure drives long-lived impairment of hematopoietic stem cell self-renewal activity and accelerated aging. Cell Stem Cell *29*, 1273–1284.e8. https://doi.org/10.1016/j.stem.2022.06.012.

82. Pinho, S., and Frenette, P.S. (2019). Haematopoietic stem cell activity and interactions with the niche. Nat. Rev. Mol. Cell Biol. *20*, 303–320. https://doi.org/10.1038/s41580-019-0103-9.

83. Höpner, S.S., Raykova, A., Radpour, R., Amrein, M.A., Koller, D., Baerlocher, G.M., Riether, C., and Ochsenbein, A.F. (2021). LIGHT/LTβR signaling regulates self-renewal and differentiation of hematopoietic and leukemia stem cells. Nat. Commun. *12*, 1065. https://doi.org/10.1038/s41467-021-21317-x.

84. Nakagawa, M.M., Chen, H., and Rathinam, C.V. (2018). Constitutive Activation of NF-κB Pathway in Hematopoietic Stem Cells Causes Loss of Quiescence and Deregulated Transcription Factor Networks. Front. Cell Dev. Biol. *6*, 143. https://doi.org/10.3389/fcell.2018.00143.

85. Fang, J., Muto, T., Kleppe, M., Bolanos, L.C., Hueneman, K.M., Walker, C.S., Sampson, L., Wellendorf, A.M., Chetal, K., Choi, K., et al. (2018). TRAF6 Mediates Basal Activation of NF-κB Necessary for Hematopoietic Stem Cell Homeostasis. Cell Rep. *22*, 1250–1262. https://doi.org/10.1016/j.celrep.2018.01.013.

86. Chen, Z., Amro, E.M., Becker, F., Hölzer, M., Rasa, S.M.M., Njeru, S.N., Han, B., Di Sanzo, S., Chen, Y., Tang, D., et al. (2019). Cohesin-mediated NF-κB signaling limits hematopoietic stem cell self-renewal in aging and

inflammation. J. Exp. Med. *216*, 152–175. https://doi.org/10.1084/jem.20181505.

87. Toghani, D., Gupte, S., Zeng, S., Mahammadov, E., Crosse, E.I., Seyedhassantehrani, N., Burns, C., Gravano, D., Radtke, S., Kiem, H.-P., et al. (2024). Semaphorin 4A maintains functional diversity of the hematopoietic stem cell pool. preprint at bioRxiv. https://doi.org/10.1101/2024.11.12.622506.

88. Newell, R., Pienaar, R., Balderson, B., Piper, M., Essebier, A., and Bodén, M. (2021). ChIP-R: Assembling reproducible sets of ChIP-seq and ATAC-seq peaks from multiple replicates. Genomics *113*, 1855–1866. https://doi.org/10.1016/j.ygeno.2021.04.026.

89. Robinson, M.D., McCarthy, D.J., and Smyth, G.K. (2010). edgeR: a Bioconductor package for differential expression analysis of digital gene expression data. Bioinformatics *26*, 139–140. https://doi.org/10.1093/bioinformatics/btp616.

90. Heinz, S., Benner, C., Spann, N., Bertolino, E., Lin, Y.C., Laslo, P., Cheng, J.X., Murre, C., Singh, H., and Glass, C.K. (2010). Simple combinations of lineage-determining transcription factors prime cis-regulatory elements required for macrophage and B cell identities. Mol. Cell *38*, 576–589. https://doi.org/10.1016/j.molcel.2010.05.004.

91. Lawrence, M., Huber, W., Pagès, H., Aboyoun, P., Carlson, M., Gentleman, R., Morgan, M.T., and Carey, V.J. (2013). Software for Computing and Annotating Genomic Ranges. PLoS Comput. Biol. *9*, e1003118. https://doi.org/10.1371/journal.pcbi.1003118.

92. Robinson, J.T., Thorvaldsdóttir, H., Winckler, W., Guttman, M., Lander, E.S., Getz, G., and Mesirov, J.P. (2011). Integrative Genomics Viewer. Nat. Biotechnol. *29*, 24–26. https://doi.org/10.1038/nbt.1754.

93. Mi, H., Muruganujan, A., and Thomas, P.D. (2013). PANTHER in 2013: modeling the evolution of gene function, and other gene attributes, in the context of phylogenetic trees. Nucleic Acids Res. *41*, D377–D386. https://doi.org/10.1093/nar/gks1118.

94. Zheng, G.X.Y., Terry, J.M., Belgrader, P., Ryvkin, P., Bent, Z.W., Wilson, R., Ziraldo, S.B., Wheeler, T.D., McDermott, G.P., Zhu, J., et al. (2017). Massively parallel digital transcriptional profiling of single cells. Nat. Commun. *8*, 14049. https://doi.org/10.1038/ncomms14049.

95. Friedman, J., Hastie, T., and Tibshirani, R. (2010). Regularization Paths for Generalized Linear Models via Coordinate Descent. J. Stat. Softw. *33*, 1–22. https://doi.org/10.18637/jss.v033.i01.

96. Butler, A., Hoffman, P., Smibert, P., Papalexi, E., and Satija, R. (2018). Integrating single-cell transcriptomic data across different conditions, technologies, and species. Nat. Biotechnol. *36*, 411–420. https://doi.org/10.1038/nbt.4096.

97. Korotkevich, G., Sukhov, V., Budin, N., Shpak, B., Artyomov, M.N., and Sergushichev, A. (2021). Fast gene set enrichment analysis. preprint at bioRxiv. https://doi.org/10.1101/060012.

98. Castanza, A.S., Recla, J.M., Eby, D., Thorvaldsdóttir, H., Bult, C.J., and Mesirov, J.P. (2023). Extending support for mouse data in the Molecular Signatures Database (MSigDB). Nat. Methods *20*, 1619–1620. https://doi.org/10.1038/s41592-023-02014-7.

99. Durinck, S., Moreau, Y., Kasprzyk, A., Davis, S., De Moor, B., Brazma, A., and Huber, W. (2005). BioMart and Bioconductor: a powerful link between biological databases and microarray data analysis. Bioinformatics *21*, 3439–3440. https://doi.org/10.1093/bioinformatics/bti525.

100. Chia, J.J., Zhu, T., Chyou, S., Dasoveanu, D.C., Carballo, C., Tian, S., Magro, C.M., Rodeo, S., Spiera, R.F., Ruddle, N.H., et al. (2016). Dendritic cells maintain dermal adipose-derived stromal cells in skin fibrosis. J. Clin. Investig. *126*, 4331–4345. https://doi.org/10.1172/JCI85740.

101. Palanichamy, J.K., Tran, T.M., Howard, J.M., Contreras, J.R., Fernando, T.R., Sterne-Weiler, T., Katzman, S., Toloue, M., Yan, W., Basso, G., et al. (2016). RNA-binding protein IGF2BP3 targeting of oncogenic transcripts promotes hematopoietic progenitor proliferation. J. Clin. Investig. *126*, 1495–1511. https://doi.org/10.1172/JCI80046.

102. Amend, S.R., Valkenburg, K.C., and Pienta, K.J. (2016). Murine Hind Limb Long Bone Dissection and Bone Marrow Isolation. J. Vis. Exp. 53936. https://doi.org/10.3791/53936.

103. Cheng, Q.J., Ohta, S., Sheu, K.M., Spreafico, R., Adelaja, A., Taylor, B., and Hoffmann, A. (2021). NF-κB dynamics determine the stimulus specificity of epigenomic reprogramming in macrophages. Science *372*, 1349–1353. https://doi.org/10.1126/science.abc0269.

104. Vierna, J., Wehner, S., Höner zu Siederdissen, C., Martínez-Lage, A., and Marz, M. (2013). Systematic analysis and evolution of 5S ribosomal DNA in metazoans. Heredity *111*, 410–421.

STAR★METHODS

KEY RESOURCES TABLE

REAGENT or RESOURCE	SOURCE	IDENTIFIER
Antibodies		
CD135 (Flt3) Monoclonal Antibody (A2F10), PerCP-eFluor 710, eBioscience™	Invitrogen	Cat# 46-1351-82; RRID:AB_10733393
CD3 Monoclonal Antibody (17A2), PerCP-eFluor 710, eBioscience™	Invitrogen	Cat# 46-0032-82; RRID:AB_1834427
Purified anti-mouse CD16/32 Antibody	BioLegend	Cat# 101302; RRID:AB_312801
PE/Dazzle™ 594 anti-mouse/human CD11b Antibody	BioLegend	Cat# 101256; RRID:AB_2563648
APC anti-mouse/human CD45R/B220 Antibody	BioLegend	Cat# 103212; RRID:AB_312997
PE/Cy7 anti-mouse Ly-6G/Ly-6C (Gr-1) Antibody	BioLegend	Cat# 108416; RRID:AB_313381
Brilliant Violet 711™ anti-mouse CD45.1 Antibody	BioLegend	Cat# 110739; RRID:AB_2562605
FITC anti-mouse CD45.1 Antibody	BioLegend	Cat# 110706; RRID:AB_313495
APC/Fire™ 750 anti-mouse CD45.1 Antibody	BioLegend	Cat# 110752; RRID:AB_2629806
Brilliant Violet 711™ anti-mouse CD45.2 Antibody	BioLegend	Cat# 109847; RRID:AB_2616859
FITC anti-mouse CD45.2 Antibody	BioLegend	Cat# 109806; RRID:AB_313443
PE anti-mouse TER-119/Erythroid Cells Antibody	BioLegend	Cat# 116208; RRID:AB_313709
PE anti-mouse CD117 (c-Kit) Antibody	BioLegend	Cat# 105808; RRID:AB_313217
PE/Cy7 anti-mouse Ly-6A/E (Sca-1) Antibody	BioLegend	Cat# 108114; RRID:AB_493596
APC/Cyanine7 anti-mouse CD48 Antibody	BioLegend	Cat# 103432; RRID:AB_2561463
APC anti-mouse CD150 (SLAM) Antibody	BioLegend	Cat# 115910; RRID:AB_493460
Brilliant Violet 711™ anti-mouse CD117 (c-Kit) Antibody	BioLegend	Cat# 105835; RRID:AB_2565956
Brilliant Violet 421™ anti-mouse Ki-67 Antibody	BioLegend	Cat# 652411, RRID:AB_2562663
Brilliant Violet 510™ Streptavidin	BioLegend	Cat# 405234; N/A
Brilliant Violet 711™ Streptavidin	BioLegend	Cat# 405241; N/A
TotalSeq-B barcode antibodies Hashtag#1	BioLegend	Cat# 155831; RRID:AB_2814067
TotalSeq-B barcode antibodies Hashtag#2	BioLegend	Cat# 155833; RRID:AB_2814068
Chemicals, peptides, and recombinant proteins		
DAPI (4′,6-Diamidino-2-Phenylindole, Dilactate)	Invitrogen	Cat# D3571; RRID:AB_2307445
eBioscience™ Fixable Viability Dye eFluor™ 506	Invitrogen	Cat# 50-246-097; N/A
Critical commercial assays		
Luminex mouse 32-plex assay	EMD Millipore	Cat# MCYTMAG-70K-PX32; N/A
MagniSort™ Mouse Hematopoietic Lineage Depletion Kit	Invitrogen	Cat# 8804-6829-74; RRID:AB_2575269
Foxp3/Transcription Factor Fixation/Permeabilization Buffer Set	eBioscience	Cat# 00-5523-00; N/A
Annexin V Apoptosis Detection Kit eFluor™ 450	eBioscience	Cat# 88-8006-74; RRID:AB_2575164
Chromium Next GEM Single Cell 3′ GEM, Library & Gel Bead Kit v3.1	10X Genomics	Cat# PN-1000121; N/A
Illumina Tagment DNA Enzyme and Buffer Small Kit	Illumina	Cat# 20034197; N/A
Nextera DNA Library Preparation Kit (24 samples)	Illumina	Cat# FC-121-1030; N/A
MinElute PCR Purification Kit (50)	Qiagen	Cat# 28004; N/A
Library Quant Kit (Illumina, Universal)	KAPA Biosystems	Cat# KK4824; N/A
Deposited data		
Murine HSPC subset bulk ATAC-sequencing data	This manuscript	GEO: GSE264569
Murine HSPC single-cell RNA sequencing data	This manuscript	GEO: GSE261946
Murine ChIP for C/EBPα	Jakobsen et al.[33]	GEO: GSM1347229
Murine ChIP for C/EBPβ	Link et al.[34]	GEO: GSM2974656

(*Continued on next page*)

Continued

REAGENT or RESOURCE	SOURCE	IDENTIFIER
Murine ChIP for C/EBPδ	Comoglio et al.[35]	GEO: GSM2663838
Murine HSPC subset sorted bulk microarray data	Pietras et al.[18]	GEO: GSE68529
Murine HSPC subset sorted single-cell RNA sequencing data	Rodriguez-Fraticelli et al.[36]	GEO: GSE90742
Murine HSPC single-cell RNA sequencing data	Mitchell et al.[41]	GEO: GSE169162
Murine HSPC single-cell RNA sequencing data	Hérault et al.[42]	GEO: GSE147729
Human CD34-positive single-cell RNA sequencing data	Ainciburu et al.[43]	GEO: GSE180298
Human CD34-positive subset sorted single-cell RNA sequencing data	Zhang et al.[44]	GEO: GSE137864
Mus musculus Genome assembly GRCm38/mm10	NCBI, UCSC	https://www.ncbi.nlm.nih.gov/datasets/genome/GCA_000001635.2/ https://genome.ucsc.edu/cgi-bin/hgGateway?db=mm10
Experimental models: organisms/strains		
Mouse: C57BL/6J	The Jackson Laboratory	JAX: 000664; RRID: IMSR_JAX:000664
Mouse: B6.SJL-*Ptprc*^{a}*Pepc*^{b}/BoyJ	The Jackson Laboratory	JAX: 002014; RRID: IMSR_JAX:002014
Mouse: RelA-mVenus (C57BL/6J background)	Adejala et al.[17]	N/A
Mouse: *Nfkbib*$^{-/-}$*Nfkbie*$^{-/-}$*Nfkbia*$^{+/-}$ (C57BL/6J background)	This manuscript	N/A
Software and algorithms		
FlowJo	TreeStar	v10.8.1; N/A
R	https://www.r-project.org	v4.3.2; N/A
ChIP-R	Newell et al.[88]	v1.1.0; N/A
EdgeR	Robinson et al.[89]	v3.3.6 (scRNA-seq), v4.0.9 (ATAC-seq); N/A
HOMER Motif Analysis	Heinz et al.[90]	v4.10.3; N/A
GenomicsRanges	Lawrence et al.[91]	v1.54.1; N/A
Integrative Genomics Viewer	Robinson et al.[92]	v2.9.4; N/A
PANTHER GO Analysis	Mi et al.[93]	https://pantherdb.org
Cellranger	Zheng et al.[94]	V7.0; N/A
glmnet	Friedman et al.[95]	v4.1-7; N/A
Seurat	Butler et al.[96]	v4.4.0; N/A
decoupleR	Badia-i-Mompel et al.[46]	v2.8.0; N/A
Fgsea	Korotkevich et al.[97]	v1.2.0; N/A
msigdb	Castanza et al.[98]	v7.5.1; N/A
bioMart	Durinck et al.[99]	v2.5.0; N/A
Code, including HSPC labeling and scRNA-sequencing analysis	This manuscript	Zenodo: https://doi.org/10.5281/zenodo.10828398

METHOD DETAILS

Mice

Young (2–3 months) and aged (18–22 months) male and female C57Bl/6 and B6.SJL-Ptprc^{a}Pepc^{b}/BoyJ (CD45.1) mice were obtained from The Jackson Laboratory and our own breeding colony. Previously described *Nfkbia* $^{\pm}$ mice[16] were bred with *Nfkbib*$^{-/-}$ and *Nfkbie*$^{-/-}$ strains[20,21] to generate "IκB^{-}" *Nfkbia*$^{+/-}$*Nfkbib*$^{-/-}$*Nfkbie*$^{-/-}$. mVenus-RelA mice were previously described.[17] Female and male mice were used; no overt differences between sexes were noted and thus sex was not considered as a biological variable. Animals were maintained and experiments conducted in accordance with protocols approved by the UCLA Institutional Animal Care and Use Committee.

Flow cytometry and cell sorting

Peripheral blood and bone marrow cells collected, processed, stained with fluorochrome-conjugated antibodies, and HSPC cell populations identified as previously described.[18,100–102] Ki67 staining performed following fixation and permeabilization (eBioscience

Cat # 00-5523-00), and Annexin V staining performed with Apoptosis detection kit (eBioscience Cat# 88-8006-74), both per manufacturer protocols. For cell sorting, lineage-positive cells were pre-depleted using Invitrogen MagniSort Mouse Hematopoietic Lineage Depletion Kit (Invitrogen, Cat#8804-6829-74) per the manufacturer protocol, with lineage-biotin antibody cocktail at 100μL/10 million cells, and SA-magnetic beads at 20μL/10 million cells. Flow cytometry performed with a LSRFortessa X-20 (BD Biosciences). Flow sorting performed with FACS AriaIII Cell Sorters (BD Biosciences). Cells counted via CytoFlex (Beckman Coulter). Analysis performed using FlowJo v10.8.1 (TreeStar).

Cell quantification from flow cytometry

To calculate cell number, the percentage of the gated population was multiplied by the absolute cell counts.[100] To calculate HSPC composition, the percentage of the gated population was calculated by dividing the number of cells within a subset (e.g., LT-HSC) by the total number of HSPCs ($Lin^-/Sca1^+cKit^{hi}$).

Histology and microscopy

Mouse sterna were formaldehyde-fixed and paraffin-embedded per standard histological protocols, then sectioned and stained with H&E. Analysis performed by a board-certified Hematopathologist (J.J.C.), and photographed using a BX43 microscope, DP27 camera and cellSens Standard 3.2 (all Olympus).

Luminex

Bone marrow from bilateral femurs was collected via centrifugation[102] in 200μL PBS; cells were resuspended in the supernatant and re-pelleted at 5000g for 3mins at 4C. Supernatants were immediately collected and stored at −80C. At the time of assay, samples were thawed, spun at 13,000xg for 10 min at 4C, and low-input format mouse 32-plex Luminex (EMD Millipore) was performed per manufacturer's protocols.

Bone marrow transplantation

Bone marrow transplantation was performed as previously described.[101] Briefly, recipient mice were lethally irradiated with a Cesium irradiator (1100 rads); 24 h later, 3–5 million total donor bone marrow cells pooled from 2 to 3 donor mice were injected retro-orbitally, resulting in a minimum of 750 combined HSCs per recipient mouse, which is above the threshold for consistent chimerism in non-competitive transplants.[24] Animals were maintained in sterile cages with sterilized food and autoclaved water for two weeks following irradiation. Thereafter, animals were maintained in autoclaved cages. Peripheral blood chimerism was evaluated at the specified time points by retro-orbital bleed.

ATAC-seq

Cell isolation and library preparation

CD45.1 donor LT-HSC, MPP2, MPP3 and MPP4 populations were sorted from WT or $I\kappa B^-$ recipients 13–15 weeks after transplantation, with 650-10,000 cells/population. Nuclei isolation, transposase reactions, and library preparation were performed as previously described,[103] separately for $n = 3$ pairs of chimeric mice.

Sequencing and pre-processing

Libraries were multiplexed and single-end sequenced with a length of 75bp on the NextSeq500 High Output sequencing system. Read trimming, alignment, filtering, duplicate removal, peak calling and browser track preparation were performed as previously described.[103] Consensus peaks (13910) were identified between biological replicates using ChIP-R v1.1.0.[88]

Analysis

Differential accessibility analysis was performed in R v4.3.2 with EdgeR v4.0.9 using TMM normalization, glmQLFit and glmTreat arguments.[89] TF accessibility analysis and peak annotations were performed using Homer v4.10.3.[90] ChIP datasets C/EBPα[33] (GEO: GSM1347229), C/EBPβ[34] (GEO: GSM2974656) and C/EBPδ[35] (GEO: GSM2663838). ATAC-seq and ChIP-seq peak overlaps identified using GenomicsRanges v1.54.1.[91] Consensus peaks visualized using Integrative Genomics Viewer v2.9.4.[92] For comparison to scRNA-seq, peaks were assigned to the nearest gene. GO analysis performed using PANTHER[93] accessed via AmiGO2 (amigo.geneontology.org; pantherdb.org).

scRNA-seq

Cell isolation and library preparation

CD45.1 donor HSPCs ($Lin^-/Sca1^+cKit^{hi}$) were sorted from WT or IκB– recipients 15 weeks after transplantation. ~30,000 HSPCs were incubated with TotalSeq-B barcode antibodies Hashtag#1 (WT recipient, Biolegend Cat#155831) and #2 ($I\kappa B^-$ recipient; Biolegend Cat#155833 respectively) per manufacturer's protocol, then pooled for sequencing. Single cell transcriptome and barcode libraries were generated using Chromium Next GEM Single Cell 3' Reagent Kits v3.1 (10X Genomics).

Sequencing and pre-processing

Libraries were paired-end sequenced with a length of 50bp on the NovaSeqSP system. Read counts were quantified using Cellranger v7.0.[94] Standard quality-control criteria based on minimum UMI, percent mitochondrial counts, and potential doublets were applied. Principal component analysis (PCA) was calculated from 115 hematopoietic genes (Table S1).

HSPC labeling model

Microarray reference data from flow-sorted LT-HSC, ST-HSC, MPP2, MPP3 and MPP4[18] was filtered by reference flow-sorted scRNA-seq data[36] identifying13522 reference probes mapping to 11644 reference scRNA-seq genes with nonzero counts in >1% of cells. A logistic regression model using glmnet v4.1-7[95] was built by subsampling 1% of filtered reference probes for 1000 iterations imposing an L1 lasso penalty, and limited to non-negative values to identify positive marker genes. The mean of the iterations was calculated yielding a final labeling coefficient matrix of 8511 probes mapping to 7563 genes. To apply the labeling model, the final coefficient matrix was multiplied by the scRNA-seq genes by cells matrix, yielding scores for all 5 cell types across every cell in the dataset. Cell-type probabilities were calculated by dividing each cell type score by the sum of all 5 scores within a single cell; the predicted cell identity was then set to the highest probability. For human datasets, ribosomal genes were excluded.[104]

Analysis

Principal components were calculated using 115 genes with established roles in hematopoiesis. DEG analysis (Figure 4) performed using Seurat v4.4.0.[96] Single cell gene set enrichment scores calculated as normalized mean rank for each gene set and z-scored by dataset.[37] TF activity estimated using decoupleR v2.8.0.[46] Aged DEG pseudobulk analysis performed by summing single cell counts in EdgeR v3.3.6 with glmFit and glmLRT, and experiments as a covariate.[89] Fgsea v1.2.0 used to generate GO ranked by logFC and collapsePathways, with terms from msigdb v7.5.1.[97,98] Human to mouse genes mapped with bioMart v2.5.0. All gene lists available in Table S1.

QUANTIFICATION AND STATISTICAL ANALYSIS

Statistical testing methodologies are specified for each analysis in the relevant figure legend. T-tests were performed in Excel (Microsoft). Wilcoxon Rank Sum tests, KS tests of the distribution, and Spearman correlations were performed in R v4.3.2. ATAC-seq TF enrichment analyses employed ZOOPS scoring in Homer v4.10.3. BH adjusted p-values for Figure 4 DEG performed using Seurat v4.4.0. BH adjusted p-values for Figure 6 generated in EdgeR v3.3.6 with glmFit and glmLRT, and experiments as a covariate. Where unreported, p-value is >0.05.